Numerical Simulation of the Blocking Process

by
Y. Kikuchi

Technical Paper No. 125
Department of Atmospheric Science
Colorado State University
Fort Collins, Colorado

Colorado State University

Department of Atmospheric Science

Paper No. 125

NUMERICAL SIMULATION OF THE BLOCKING PROCESS

by

Y. Kikuchi [1,2]

Department of Atmospheric Science
Colorado State University
Fort Collins, Colorado

June 1968

Atmospheric Science Paper No. 125

1) On leave from Meteorological Research Institute, Tokyo, Japan
2) This report was prepared and the research supported in part with funds administered by the National Science Foundation, Grant No. GA-761.

CONTENTS

Numerical Simulation of the Blocking Process

by

Y. Kikuchi

Colorado State University

ABSTRACT

The geostrophic system of equations with both the effects of orography and heat contrast corresponding to land-sea distribution is integrated with respect to time by using the spectral method. The computed results show the appearance of reasonable blocking situation and a corresponding double jet stream in the latitudinal distribution of the zonally averaged zonal wind.

The budgets of heat, angular momentum and energy for the period characterized by the predominant double jet stream are compared with those for another period to clarify the dynamical properties concerning blocking. The results of comparison are summarized as follows:

1. As a result of the unusual poleward transport of heat, the meridional circulation has a 4-cell structure for the period during which the double jet stream predominates.

2. In the upper layer, the angular momentum is transferred to high latitudes to compensate for the destruction of angular momentum due to the direct polar meridional circulation, forming a 4-cell structure during this period. This angular momentum contributes to the formation and development of the north branch of the double jet stream.

3. The poleward transports of heat and angular momentum are performed mainly by the disturbance of wave number 2 which shows a large growth when the predominant double jet stream appears.

4. In the upper layer, this disturbance is fed by conversion of available potential energy into kinetic energy through the baroclinic process and by transport of kinetic energy from the lower layer through the pressure force; while, in the lower layer, mainly by the transformation from zonal to eddy kinetic energy through the effect of mountains.

5. The difference between the diabatic heatings of the oceans and the continents becomes smaller during the predominant blocking situation.

1. Introduction

We frequently observe that a zonal flow breaks down into cellular motions constituted of intense and warm anticyclones or ridges with cyclones to the south. In consequence, a jet stream is blocked by these vortices and splits into two branches, one of which is located to the north of the anticyclone and the other to the south of the cyclone. The characteristics of this blocking situation are persistence and quasi-stationarity, and occurrence at rather well-defined longitudes.

This phenomenon, which was first noted by Garriott (1904), aroused the interest of many investigators because of its pronounced influence upon the weather and climate. Namias (1947), Elliott and Smith (1949), Berggren, Bolin and Rossby (1949), Rex (1950a) and many others have presented its synoptic description. On the other hand, the theoretical explanation of the phenomenon was attempted by Yeh (1949), Rossby (1950), Rex (1950a) and Thompson (1957). In these tentative theories, however, it should be noted that the blocking was considered as a barotropic process.

As well-known, owing to the recent development of the electronic computer, accompanied by the progress of the computation technique and the refinement of atmospheric models, many numerical experiments have been made on the general circulation. (For example, as recent investigations, Mintz (1964), Smagorinsky, Manabe and Holloway (1965), Manabe, Smagorinsky and Strickler (1965), and Kasahara and Washington (1967).) However, a numerical experiment which pays special attention to the blocking phenomenon has not yet been attempted.

The facts that the scales of the blocking phenomenon are very large and the places of its occurrence are well defined make us imagine that the orography and the heat contrast due to the land-sea distribution would play important roles in the blocking process. This inference seems to be unquestionable because the blocking processes have never yet been produced by the numerical experiments using the atmospheric models without consideration of the orography and the land-sea distribution.

Although, according to Burger's scale analysis (1958), the vorticity equation applied to the waves of such planetary size as blocking waves looses the prognostic character, Deland (1965) has recently indicated that the vorticity equation applicable to the cyclone waves may also be applied to the ultra-long waves. Thus, it would be significant to examine whether the blocking phenomenon can be governed by the geostrophic vorticity equation.

In this paper, the first aim is to perform the numerical simulation of the blocking process by the use of the geostrophic system of equations, including both effects of the orography and the contrast heating due to land-sea distribution. The second aim is to clarify the dynamical characteristic features concerning the blocking process through analysis of the results obtained.

2. Construction of Model

A. Governing Equations

In this study, we will assume that the change in the state of the atmosphere is given by the vorticity equation with the friction term

$$\frac{\partial \nabla^2 \psi}{\partial t} + J(\psi, \nabla^2\psi + f) + \nabla(f\nabla\chi) = F \qquad (1)$$

the thermodynamic equation with the heat diffusion and non-adiabatic heating terms

$$\frac{\partial T}{\partial t} + J(\psi, T) - \frac{p}{R}\sigma\omega = B + \frac{q}{Cp} \qquad (2)$$

and the thermal wind equation

$$\nabla^2 T = -\frac{p}{R}\nabla\cdot(f\nabla\frac{\partial\psi}{\partial p}) \qquad (3)$$

which is derived from the geostrophic approximation

$$\nabla^2\Phi = \nabla\cdot(f\nabla\psi) \qquad (4)$$

Pressure is adopted as the vertical coordinate, the static stability

$$\sigma = -\alpha_s \frac{\partial \ln\theta_s}{\partial p}$$

is taken to be $3.0 m^2 sec^{-2} cb^{-2}$ and, considering the spherical earth,

$$f = 2\Omega \sin\phi$$

$$\nabla = i \frac{\partial}{a \cos\phi \, \partial\lambda} + j \frac{\partial}{a\partial\phi}$$

$$\nabla^2 = \frac{1}{a^2 \cos\phi}\left[\frac{1}{\cos\phi}\frac{\partial^2}{\partial\lambda^2} + \frac{\partial}{\partial\phi}\left(\cos\phi \frac{\partial}{\partial\phi}\right)\right]$$

$$J(A,B) = \frac{1}{a^2 \cos\phi}\left(\frac{\partial A}{\partial\lambda}\frac{\partial B}{\partial\phi} - \frac{\partial A}{\partial\phi}\frac{\partial B}{\partial\lambda}\right)$$

The notations used in the above equations are as follows:

t - time
p - pressure
λ - longitude
ϕ - latitude
ψ - stream function
Φ - geopotential height on an isobaric surface
χ - velocity potential of divergent part of wind
T - absolute temperature
ω - vertical p-velocity
F - rate of vorticity change due to momentum diffusion by small-scale eddies.
B - rate of temperature change due to lateral heat diffusion by small-scale eddies.
q - rate of non-adiabatic heating per unit air mass

α_s - standard value of specific volume
θ_s - standard value of potential temperature
f - Coriolis parameter
R - gas constant for dry air
Cp - specific heat of air at constant pressure
a - radius of earth
Ω - angular velocity of earth
i,j - eastward and northward unit vectors, respectively

The differences between the system of equations (1)-(3) and the so-called quasi-geostrophic system of equations are to treat the Coriolis parameter as a function of latitude in equations (1) and (3), and to include the term $\nabla\chi\cdot\nabla f$ representing the advection of vorticity of the earth's rotation by the divergent part of wind in the vorticity equation (1). This term is necessary to guarantee that the system of equations (1)-(3), ignoring the diffusion and non-adiabatic heating terms, is energy conserving when the Coriolis parameter is variable. [See Lorenz (1960)]

For convenience, we introduce the new variable x defined by

$$X = -\int_0^p \chi\, dp'$$

so that

$$\chi = -\frac{\partial X}{\partial p} \qquad (5)$$

$$\omega = \nabla^2 X \qquad (6)$$

Since we will consider the atmospheric motion in the troposphere, 200- and 1000- mb surfaces are taken as the upper and lower boundaries of our model atmosphere, respectively. In our model, the atmosphere is divided into two layers by the 600- mb surface. We will apply the vorticity equation at 400- and 800- mb surfaces and the thermodynamic and thermal wind equations at the 600- mb surface. Then, considering equations (5) and (6), the governing equations may be rewritten as follows:

$$\frac{\partial}{\partial t}\nabla^2\psi_1 + J(\psi_1, \nabla^2\psi_1 + f) + \frac{1}{\Delta p}\nabla[f\nabla(X_2-X_0)] = F_1 \qquad (7)$$

$$\frac{\partial}{\partial t}\nabla^2\psi_3 + J(\psi_3, \nabla^2\psi_3 + f) + \frac{1}{\Delta p}\nabla[f\nabla(X_4-X_2)] = F_3 \qquad (8)$$

$$\frac{\partial}{\partial t}T_2 + J(\psi_2, T_2) - \frac{p_2}{R}\sigma\nabla^2 X_2 = B_2 + \frac{g}{2C_p\,\Delta p}Q \qquad (9)$$

$$\nabla^2 T_2 = -\frac{p_2}{R\Delta p}\nabla[f\nabla(\psi_1-\psi_3)] \qquad (10)$$

where Q is the rate of non-adiabatic heating in the air column of unit cross-section,

$$\psi_2 = \frac{1}{2}(\psi_1 + \psi_3)$$

$$\Delta p = p_2-p_0 = p_4-p_2$$

and the subscripts 0, 1, 2, 3, and 4 refer to the quantities at 200-, 400-, 600-, 800-, and 1000- mb levels as shown in Fig. 1, respectively.

B. Diffusion Due to Small-Scale Eddies

The rate of vorticity change due to momentum diffusion by small-scale eddies, i.e. friction term, may be separated into two parts as follows:

$$F = M + N$$

where the friction term due to horizontal diffusion M and that due to vertical diffusion N will be given by

$$M = A_M \nabla^2 (\nabla^2\psi + \frac{2\psi}{a^2}) \qquad (11)$$

$$N = -g \frac{\partial \tau}{\partial p} \tag{12}$$

Here A_M is the lateral kinetic eddy-viscosity coefficient, g the acceleration of gravity and τ the rotation of stress acting across the horizontal surface. The last term in the equation (11) results from the effect of the spherical earth. The rotation of the stress due to vertical diffusion is taken as

$$\tau = - \mu g \rho \frac{\partial \nabla^2 \psi}{\partial p} \tag{13}$$

where ρ is the density, μ the small-scale vertical eddy stress coefficient.

If equations (11) and (12) are applied at the levels 1 and 3 corresponding to equations (7) and (8), we obtain the following forms:

$$M_j = A_M \nabla^2 (\nabla^2 \psi_j + \frac{2\psi_j}{a^2}) \quad (j = 1,3) \tag{14}$$

$$N_1 = \frac{g}{\Delta p} (\tau_0 - \tau_2) \tag{15}$$

$$N_3 = \frac{g}{\Delta p} (\tau_2 - \tau_4) \tag{16}$$

Applying equation (13) at level 2, we have the following difference form for τ_2:

$$\tau_2 = \frac{\Delta p}{g} k_i (\nabla^2 \psi_1 - \nabla^2 \psi_3) \tag{17}$$

where the coefficient, $k_i = \mu \rho (\frac{g}{\Delta p})^2$, is taken to be 0.5×10^{-6} sec^{-1} as was used by Charney (1959) and Mintz (1964). With respect to τ_0 and τ_4, we will assume as follows:

$$\tau_0 = 0 \tag{18}$$

$$\tau_4 = \frac{\Delta p}{g} k_s \nabla^2 \psi_4 \tag{19}$$

where $k_s = 4 \times 10^{-6} sec^{-1}$ and ψ_4 is estimated by the linear extrapolation from the levels 1 and 3. Eqs. (18) and (19) are ones of the vertical boundary conditions and have been used by Phillips (1956) and other investigators.

Since the whole atmosphere is treated as one layer with respect to its thermal state, only lateral diffusion will be considered as the process for redistribution of heat due to eddy diffusion. The temperature change due to lateral heat diffusion is given by

$$B = A_T \nabla^2 T$$

where A_T is the lateral eddy-diffusion coefficient. As performed by Phillips (1956), it will be assumed that

$$A_T = A_M = A = 10^5 m^2 sec^{-1}$$

Corresponding to the Eq. (9), B_2 is written as

$$B_2 = A \nabla^2 T_2 \qquad (20)$$

C. Heating Function

In the thermodynamic Eq. (9), the rate of the non-adiabatic heating Q may be separated into three parts as follows:

$$Q = Q_{SR} + Q_{LR} + Q_{CS} \qquad (21)$$

where Q_{SR}, Q_{LR} are the rates of heating of an air column with unit cross-section due to the absorption of short-wave and long-wave radiation, respectively, and Q_{CS} is that due to condensation in the atmosphere and sensible heat transferred from the earth's surface to the atmosphere.

Adem's method (1962, 1964) will be used to evaluate the radiational heating. The details of the method are described in his paper. Hence only the brief outline is given here.

With respect to long-wave radiation, it is assumed that the atmosphere is transparent for the wave length from 8μ to 13μ, while behaving as a black body for the other wave lengths. Therefore, the energy emitted by a unit area of boundary of the atmospheric layer of the temperature T or, when the radiation emitted by a unit area of the surface of a black body of the temperature T passes through the atmosphere, the energy absorbed by the atmosphere is given by

$$E(T) = \sigma T^4 - F(T) \tag{22}$$

where σT^4 is the energy emitted by unit area of the surface of a black body of temperature T and F(T) is that part contained in the region of transparency.

Using the notations E(T) and F(T), at the top and bottom of the atmosphere, the net upward long-wave radiations per unit area, L_T and L_E, are given by

$$L_T = (1-\varepsilon)\, F(T_s) + E(T - \frac{\beta}{2} H) + \varepsilon F(T_c) \tag{23}$$

$$L_E = \alpha T_s^4 - E(T + \frac{\beta}{2} H) - \varepsilon F(T_c) \tag{24}$$

where T_s is the temperature of the earth's surface, T_c=261°K the temperature of cloud, ε=0.5 the ratio of cloud cover, β=6.5°K km^{-1} the lapse rate of the atmospheric temperature, T the mean atmospheric temperature, H the height of the atmosphere, $T-\frac{\beta}{2} H$ and $T+\frac{\beta}{2} H$ the temperatures at the top and bottom of the atmosphere, respectively. Eq. (23) shows that upward long-wave radiation at the top of the atmosphere is composed of the window radiation emitted by the earth's surface, which is partly absorbed by clouds, radiation emitted by the upper boundary of the atmosphere and the window radiation emitted from clouds to space. The net upward radiation at the bottom of the atmosphere is given by the difference between upward radiation from the earth's surface and downward radiation from the bottom of the atmosphere plus the downward window radiation from cloud to earth.

In order to linearize Eqs. (23) and (24), we separate T_s, T and H into the constant parts and the deviative parts as follows:

$$T_s = \overline{T_s} + T_s'$$

$$T = \overline{T} + T'$$

$$H = \overline{H} + H'$$

As a result of linearization, Eqs. (23) and (24) may be written as follows:

$$L_T = a_0 + a_1 T_s' + a_2 T' \qquad (25)$$

$$L_E = b_0 + b_1 T_s' + b_2 T' \qquad (26)$$

where H' is eliminated by

$$H' = T' \frac{2\overline{H}}{4\overline{T} - \beta\overline{H}}$$

Here, if $\overline{T_s}$=288°K, $\overline{T}$=255.5°K and $\overline{H}$=10^6cm are adopted, we have

$$a_0 = 436.7 \text{ ly/day}$$
$$a_1 = 2.187 \text{ ly/day K}$$
$$a_2 = 3.719 \text{ ly/day K}$$
$$b_0 = 181.0 \text{ ly/day}$$
$$b_1 = 11.296 \text{ ly/day K}$$
$$b_2 = 8.335 \text{ ly/day K}$$

Since the difference L_E-L_T is equal to the amount of heat added to the atmospheric column with unit cross-section through the long-wave radiation, Q_{LR} is represented by

$$Q_{LR} = (b_0-a_0) + (b_1-a_1)T_s' + (b_2-a_2)T' \qquad (27)$$

Due to solar radiation, the atmospheric column with unit cross-section is heated as follows:

$$Q_{SR} = (\alpha_a + \varepsilon\alpha_c)I \tag{28}$$

where α_a=0.15 and α_c=0.04 are the rates of absorption of solar radiation by the atmosphere and cloud, respectively. In this study, the insolation I, which is estimated by the Milankovitsch's formula, will be fixed to the state on January 22nd.

The rate of heating due to condensation and sensible heat from the earth's surface, Q_{CS}, will be evaluated by an empirical formula. In general, it may be considered that the rate of heating due to these effects depends upon the static stability of the atmosphere. Since the temperature is measured at two levels, i.e. 600- mb surface and the earth's surface, in our model, the static stability may be represented by the difference between the temperatures of these levels. Thus, an effort will be made to construct an empirical formula for Q_{CS} as a function of this temperature difference.

In Fig. 2, the annual mean relationship between the zonal means of the Q_{CS} and the 600- mb to the earth's surface temperature difference is shown by solid circles at every 10 degrees of latitude, starting with 5°N. For convenience, Q_{CS}'s are plotted versus the deviation of the 600- mb to the earth's surface temperature difference from its hemispheric mean, instead of the temperature difference itself.

According to this figure, Q_{CS} is expressed by the linear function of the 600- mb to earth's surface temperature difference with good approximation except the region of 15°-35°N latitude. Thus, we will adopt the following empirical formula for Q_{CS}:

$$Q_{CS} = C_N + c[(T_s - T) - \Gamma_m] \tag{29}$$

where Γ_m=18.6 is the hemispherical mean of T_s-T and C_N and c are determined from Fig. 2 to be

$$C_N = 210 \text{ ly day}^{-1}$$

and

$$C = 16.667 \text{ ly day}^{-1}\text{K}^{-1}$$

Rewriting Eq. (29) in terms of T_s' and T', we obtain

$$Q_{CS} = C_0 + C_1 T_s' + C_2 T' \tag{30}$$

where C_0=441.7 ly/day, C_1=16.667 ly/day K and C_2=$-C_1$.

Substituting (27), (28), and (30) into (21), the equation for Q is obtained as

$$Q = (\alpha_a + \varepsilon\alpha_c)I + (b_0+c_0-a_0) + (b_1+c_1-a_1)T_s' + (b_2+c_2-a_2)T' \tag{31}$$

T_s in Eq. (31) is determined by the lower boundary condition which will be assumed as follows:

1) On the sea, T_s will be given January normal values.
2) On land and ice, T_s is determined from the requirement of heat balance at the surface.

Assuming that the heat capacity of land and ice is zero, the condition of heat balance per unit area of the surface may be written as follows

$$S_E = L_E + E_{LS} \tag{32}$$

where S_E is the net downward insolation and E_{LS} the flux of latent and sensible energy transferred from the earth's surface to the atmosphere. At the top of the atmosphere, the net downward insolation S_T may be written as follows

$$S_T = (1-\gamma)I \tag{33}$$

where γ is the planetary albedo given by Fedseev's empirical formula:

$$\gamma = 0.34 + 0.11\left(\frac{9}{45} - 1\right)^2 + 0.15\left(\frac{9}{45} - 1\right) \tag{34}$$

Since the absorption of solar radiation by the atmosphere is given by Eq. (28), the net downward insolation at the earth's surface is

$$S_E = (1-\alpha_a-\varepsilon\alpha_c-\gamma)I \tag{35}$$

With respect to E_{LS}, we will assume as follows:

$$E_{LS} = Q_{CS} \tag{36}$$

Substituting (26), (35), and (36) to (32) and using (30), the condition of heat balance may be rewritten as follows:

$$(1-\alpha_a-\varepsilon\alpha_c-\gamma)I = (b_0+c_0) + (b_1+c_1)T_s' + (b_2+c_2)T' \tag{37}$$

Eq. (37) is one of the lower boundary conditions applied on land and ice. If T_s' in Eq. (31) is eliminated with use of Eq. (37), Q over land and ice is evaluated by the atmospheric temperature alone. Thus, we have the following heating function:

$$Q = E(\lambda,\phi)-G(\lambda,\phi)T' \tag{38}$$

where E and G are known functions of λ and ϕ given by

$$E = (1-\alpha_a-\varepsilon\alpha_c-\gamma)I+(b_0+c_0-a_0)+(b_1+c_1-a_1)T_s' \quad \text{and}$$

$$G = -(b_2+c_2-a_2) \quad \text{on the sea,}$$

$$E = (1-\alpha_a-\varepsilon\alpha_c-\gamma)I+(b_0+c_0-a_0)+(b_1+c_1-a_1)\frac{(1-\alpha_a-\varepsilon\alpha_c-\gamma)I-b_0-c_0}{b_1+c_1}$$

$$\text{and } G = (b_1+c_1-a_1)\frac{b_2+c_2}{b_1+c_1} - (b_2+c_2-a_2) \quad \text{on land and ice.}$$

The distribution of E is shown in Fig. 4a. In Fig. 4b, the distribution of E is shown reproduced by the truncated series which will be used for time integration of the governing equations as will be described later. This is the distribution of E used in the actual calculation.

D. Boundary Conditions

As the lateral boundary condition, it will be assumed that the velocity and temperature fields are symmetric with respect to the equator. This means that hemispherical interaction is ignored.

We have already described the vertical boundary conditions concerning the friction and non-adiabatic heating terms. Here the remaining vertical boundary conditions concerning X will be described.

At the top of the atmosphere, the following condition is assumed

$$X = 0 \tag{39}$$

At the bottom of the atmosphere, we will introduce the effect of orography by giving the following condition to X:

$$\nabla(f\nabla X) = f_0\rho_s gJ(h,\psi_3) \tag{40}$$

where f_0 is the Coriolis parameter at 45°N, ρ_s the density near the earth's surface, h the height of the orography. The distribution of orographic height used in this study is shown in Fig. 5.

E. Spectral Form of Governing Equations

From the preceding discussion, we may obtain the following final expression for the governing equations:

$$\frac{\partial}{\partial t}\nabla^2\psi_1+J(\psi_1,\nabla^2\psi_1+f)-\nabla\left(f\nabla\frac{X_2}{\Delta p}\right) = A\nabla^2\left(\nabla^2\psi_1+\frac{2\psi_1}{a^2}\right)-k_i(\nabla^2\psi_1-\nabla^2\psi_3) \tag{41}$$

$$\frac{\partial}{\partial t}\nabla^2\psi_3+J(\psi_3\ \nabla^2\psi_3+f)+\nabla\left(f\nabla\frac{X_2}{\Delta p}\right)-\gamma_m J(h,\psi_3) = \tag{42}$$

$$= A\nabla^2\left(\nabla^2\psi_3+\frac{2\psi_3}{a^2}\right)+k_i(\nabla^2\psi_1-\nabla^2\psi_3)-k_s\nabla^2\psi_4$$

$$J_{\alpha\beta\gamma} = \delta^{m_\alpha}_{m_\beta+m_\gamma} \frac{1}{2} \int_{-\frac{\pi}{2}}^{\frac{\pi}{2}} p_\alpha \left(m_\beta p_\beta \frac{\partial p_\gamma}{\partial \phi} - m_\gamma p_\gamma \frac{\partial p_\beta}{\partial \phi}\right) d\phi$$

$$\delta^\alpha_\beta = \begin{cases} 0 & (\text{if } \alpha \neq \beta) \\ 1 & (\text{if } \alpha = \beta) \end{cases}$$

$$H_{\alpha\beta\gamma} = \frac{D_\beta - D_\gamma}{D_\alpha} J_{\alpha\beta\gamma}$$

$$\tau_{\alpha\gamma} = \gamma_m \frac{1}{D_\alpha} \sum_\beta h_\beta J_{\alpha\beta\gamma}$$

$$\nu_{ac} = \sum_b G_b C_{abc}$$

$$C_{abc} = \delta^{m_a}_{m_b+m_c} \frac{1}{2} \int_{-\frac{\pi}{2}}^{\frac{\pi}{2}} p_a p_b p_c \cos\phi \, d\phi$$

h_β, G_b, E_a are the complex coefficients of spherical harmonic expansion of h, G and E, respectively. For convenience, the spectral equations (48)-(51) are reduced to the non-dimensional forms by using the earth's radius, the reciprocal of the speed of the earth's angular rotation and 80-cb, which is the thickness of our model atmosphere, as the unit of length, time and pressure, respectively. We can verify that the conservative properties, i.e., energy conservation and angular momentum conservation, etc., which the original differential equations possess, are also satisfied by these spectral equations.

Substituting Eqs. (48), (49) and (50) into Eq. (51) differentiated with respect to time, a diagnostic equation concerning X, which will be called the X-equation, may be obtained. In the time integration, the vorticity equations (48) and (49) are used as the prognostic equations, while the X-equation and thermal wind relation (51) as the diagnostic equations. However, since only the component $T^\circ_\circ$ cannot be evaluated by using Eq. (51), the thermodynamic equation (50) is employed for fore-

casting this component of temperature.

3. Initial Conditions and Time Integration

The initial condition adopted for the time integration is a resting isothermal atmosphere of 258°K which is the normal winter temperature at the middle latitude of the 600mb level.

The time integration is initiated with the forward difference method (Euler method) over the interval $\frac{\Delta t}{2}$, followed by the centered difference method (leap-frog method) to Δt, thereby establishing the condition necessary to use the centered difference method for the successive time integration. To prevent nonlinear instability which will occur due to growth of the computational mode in using the centered difference method, the initiation method (mentioned above) is applied every 5 days in the course of time integration. With respect to the diffusion terms, however, the forward difference method is used to guarantee computational stability. The time interval adopted for the integration is two hours.

The time integration was performed over 130 days. Fig. 6 shows the time variations of hemispheric mean temperature, hemispheric mean relative angular momentum, total and zonal available potential energy and total and zonal kinetic energy. According to this figure, it takes about 40 days before these quantities reach the state of quasi-equilibrium. The 60-day period from 71 to 130 days was adopted for our detailed analysis of the results.

From a glance at this figure, although we can recognize the variation of zonal available potential energy with a period of approximately 40 days, it is difficult to find a distinct period in the fluctuations of the other quantities.

4. Characteristic Features of Results

In this section, we will describe some characteristic features of the computed results. Special attention will be paid to the simulation of the blocking phenomenon and its reasonableness.

A. Time Variation of Latitudinal Distribution of Zonally Averaged Zonal Current.

In Fig. 7, the time variation of the latitudinal distribution of the zonal mean of the zonal current at the upper level of the model atmosphere is shown. One feature seen in this figure is that the latitude of the subtropical jet stream has large changes with time as observed in the actual atmosphere (See, for example, Fig. 9). At times, the range of the fluctuation reaches approximately 15 degrees of latitude. Another feature is that the secondary maximum of the zonally averaged zonal wind, the latitude of which is indicated by a small solid circle in the figure, appears occasionally in high latitudes. This double jet structure indicates the appearance of the predominant blocking situation splitting a zonal current into two branches. The short lines above the figure indicate the duration of the double jet structure with the numbers representing duration in days. The longest period is 11 days from the 83rd day to the 93rd day and during this period the wind velocity of the secondary maximum is so large as to reach 18 m/sec at its maximum. Before proceeding with a discussion of reasonableness of these computed results, it is necessary to understand the observed situation of a double jet structure in the actual atmosphere.

The upper and lower parts of Fig. 8 show the annual variation of the 5-day mean zonally averaged zonal wind at the 500mb level for the years 1965 and 1966, respectively. From this figure, we can see that the double jet stream appears persistently during almost the whole period from June to July in each year. This persistent double jet stream results from the predominant blocking situation during the rainy season over the Far East. Another period during which relatively persistent double jet structures appear is the winter season. Because the insolation is fixed to the state of winter in this study, the observed results which compare with the computed results are those of the winter season.

To understand the double jet structure during the winter season in more detail, the daily variation of the zonally averaged 500 -mb zonal wind during the periods December 1964 through March 1965 and December 1965 through March 1966 is shown in the upper and lower parts of Fig. 9, respectively. According to this figure, the duration of a double jet stream is usually a week or so, but sometimes two or three weeks. The largest wind velocity of the secondary maximum of the zonally averaged zonal wind is about 18 m/sec. With respect to the duration of double

jet streams and the velocity of their north branches, we see that the computed results are in good agreement with observation by comparing Fig. 9 with Fig. 7. It is of interest that the latitude of the north branch of the double jet stream varies from year to year. The computed results compare to the case of 1966.

B. Synoptic Manifestation

In order to examine the reasonableness of the synoptic situation of blocking corresponding to the double jet structure, Fig. 10 and Fig. 11 were prepared showing the 5-day mean computed streamlines of the upper level for the periods 89-93 days and 121-125 days, both of which occur during a double jet structure. In both figures, the blocking situations occur over England and European Russia where a high frequency of blocking occurs as found by many authors [e.g., Rex (1950b), Berry, Haggard and Wolff (1954) and Serebreny, Wiegman and Hadfield (1957)].

In Fig. 12, to see the evolution of the blocking process, the daily charts of the computed streamlines at the upper level during the period 119-127 days, which includes the period used to construct Fig. 11, are displayed at 2-day intervals. Although the simulated blocking process found over England and Western Europe seems to be relatively simple, the broad features of its development are in good agreement with those of blocking in February 1948 analyzed by Berggren, Bolin and Rossby (1949). Also, the behavior of a cut-off high over Alaska in the same chart is frequently seen in the actual winter atmosphere.

Furthermore, to examine the reasonableness of the general situation of flows, the 30-day mean chart of the computed streamlines from 101 to 130 days, shown in Fig. 13, is compared with the 30-day mean 500 -mb contour heights of December 1958 in Fig. 14. The latter figure was chosen as an example of an observed flow pattern similar to that of Fig. 13. These two flow patterns are very similar to each other, especially with respect to the positions of troughs and ridges in high latitudes. Thus, it turns out that the computed flow patterns are reasonable by comparison with observation.

In the following discussion, to clarify the characteristic features concerning the blocking process causing predominant double jet structures in the latitudinal distribution of the zonally averaged zonal wind, the

60-day period chosen for detailed analysis will be divided into two 30-day periods, i.e., the first half period from 71 days to 100 days characterized by the appearance of the predominant double jet stream as shown in Fig. 7 and the latter half remaining period from 101 days to 130 days. The analyzed results for these two periods will be compared with each other.

5. State of Quasi-Equilibrium

In the upper and lower parts of Fig. 15, the 30-day mean latitude-height distributions of the zonally averaged zonal current are shown for the periods of 71-100 days and of 101-130 days, respectively. According to this figure, west winds are predominant in high latitudes of the lower layer for the first half period, while east winds predominate for the latter half period. In Fig. 16, the latitudinal distribution of the zonally averaged zonal wind at the 400 -mb level for the latter half period is compared with the observational winter mean distribution (indicated by solid circles) obtained by Mintz (1954). Although the latitude of the jet obtained from our model nearly coincides with the observation, its intensity is stronger than the observed.

In the upper and lower parts of Fig. 17, the 30-day mean latitudinal distributions of the zonal mean temperature are shown by solid lines for the first half and latter half periods, respectively. From this figure, we can see that the pole to equatorial difference of the zonal mean temperature is somewhat smaller for the first half period, during which the predominant double jet structure is found. By comparing with the observed values, which are obtained by Burdecki (1955), plotted by solid circles in the lower part of Fig. 17, it turns out that the computed temperature difference between pole and equator is about 10°C larger than observed.

The upper and lower parts in Fig. 18 show the 30-day mean latitudinal distributions of the zonal mean vertical p-velocity for the first half and latter half periods, respectively. There exists a large difference; that is, a 4-cell mean meridional circulation is formed for the first half period, characterized by the predominant double jet structure, while a 3-cell mean meridional circulation appears for the latter half period. According to the lower part of Fig. 18, in which the winter mean values of vertical

p-velocity obtained by Mintz and Lang (1955) are plotted by solid circles, the magnitude of the computed vertical p-velocity is comparable with the observed.

6. Heat Balance

Zonally averaging the thermodynamic equation (43), in consideration of equations (6) and (38), we may obtain the following equation for the change of the zonal mean temperature,

$$\frac{\partial \overline{T_2}}{\partial t} = -\frac{\overline{\partial v_2 T_2}\cos\phi}{a\cos\phi\,\partial\phi} + \frac{p_2}{R}\overline{\sigma\omega_2} + A\frac{1}{a^2\cos\phi}\frac{\partial}{\partial\phi}\left(\cos\phi\frac{\partial \overline{T_2}}{\partial\phi}\right) + \frac{g}{2\Delta p C_p}\overline{Q} \tag{52}$$

where $(\bar{\ })$ indicates the zonal mean, i.e.,

$$(\bar{\ }) = \frac{1}{2\pi}\int_0^{2\pi}(\ )\,d\lambda$$

The first and third terms on the right side of the above equation describe the rate of the zonal mean temperature change due to the convergence of heat transported by large-scale eddies, and small-scale eddies, respectively. The second and fourth terms are the rate of temperature change due to the adiabatic heating by mean vertical motions and to the diabatic heating, respectively.

According to the computed results the effective processes in the heat balance of our model atmosphere are the convergence of heat flux by large-scale eddies, the diabatic heating and the adiabatic heating by mean vertical motions. The transport of heat by small-scale eddies plays a minor role in the heat balance as pointed out in other numerical experiments of the general circulation. [See, for example, Smagorinsky, Manabe and Holloway (1965)].

In the upper and lower parts of Fig. 19, the 30-day mean latitudinal distributions of the rate of the zonal mean temperature change due to the convergence of eddy heat flux and the diabatic heating are shown for the first half and latter half periods, respectively. In the figure, the rate

of temperature change due to the diabatic heating indicated by solid lines is measured as positive upward, while that due to the convergence of eddy heat flux, indicated by dashed lines, is measured as positive downward. Therefore, the areas enclosed by solid and dashed lines represent the net effect of these two processes. Since, in the long-term average, the heating due to this net effect is almost compensated for by the adiabatic heating due to vertical motions, the upward motions appear in the warming regions denoted by W in the figure, while downward motions are in the cooling regions denoted by C. Thus, from this figure, we may understand why the 4-cell mean meridional circulation appearing for the first half period is replaced by three cells for the latter half period as described in section 5. Furthermore, according to the upper part of Fig. 19, the most northern indirect cell forming the 4-cell meridional circulation for the first half period as seen in the upper part of Fig. 18 occurs to compensate for warming caused by the intense eddy transport of heat to the polar region. For comparison, in the lower part of Fig. 19, the January mean values of the rate of temperature change due to the eddy transport of heat obtained by Wiin-Nielsen, Brown and Drake (1963) and those due to the diabatic heating obtained by Asakura and Katayama (1964) are plotted by triangle and cross symbols, respectively.

The left and right sides of Fig. 20 show the 30-day mean latitudinal distributions of the rate of the zonal mean temperature change due to convergence of heat flux for each of wave numbers 1 through 8 for the first half and latter half periods, respectively. From this figure, it turns out that the intense poleward eddy transport of heat consistent with the appearance of the indirect meridional circulation in the polar region for the first half period is performed mainly by the disturbance of wave number 2.

7. Angular Momentum Balance

If we operate on Eqs. (41) and (42) with

$$\frac{1}{2\pi}\int_{\phi}^{\frac{\pi}{2}}\int_{0}^{2\pi}(\ )\,a^2\cos\phi\;\;d\phi d\lambda$$

the following equations for angular momentum of our model may be obtained

as

$$\frac{\partial a \cos\phi\, \overline{u_1}}{\partial t} = -\frac{\partial \overline{u_1 v_1}\, \cos^2\phi}{\cos\phi\, \partial\phi} + a\cos\phi\, f\overline{v_1}' - k_i\, a\cos\phi\,(\overline{u_1}-\overline{u_3})$$

$$+A\frac{\partial}{\cos\phi\,\partial\phi}\left(\cos^2\phi\,\frac{\partial \overline{u_1}}{a\partial\phi} + \frac{\sin\phi\cos\phi}{a}\,\overline{u_1}\right) \tag{53}$$

$$\frac{\partial a \cos\phi\, \overline{u_3}}{\partial t} = -\frac{\partial \overline{u_3 v_3}\cos^2\phi}{\cos\phi\,\partial\phi} - a\cos\phi\, f\overline{v_1}' + k_i\, a\cos\phi(\overline{u_1}-\overline{u_3})$$

$$+A\frac{1}{\cos\phi}\frac{\partial}{\partial\phi}\left(\cos^2\phi\,\frac{\partial \overline{u_3}}{a\partial\phi} + \frac{\sin\phi\cos\phi}{a}\,\overline{u_3}\right) - k_s\, a\cos\phi\,\overline{u_4} - \gamma_m \overline{\psi_3 \frac{\partial h}{\partial\lambda}} \tag{54}$$

where $\overline{v_1}'$ is the velocity of the upper meridional flow of the zonal mean meridional circulation, the vertical flow of which has the zonal mean vertical p-velocity, and $\bar{}$ describes the zonal mean. The first and third terms on the right side of the equations represent the convergence of relative angular momentum flux by large-scale eddies and small-scale lateral eddy diffusion, respectively. The second and fourth terms are the rate of the exchange of relative angular momentum between the upper and lower layers resulting from the conversion between the earth's angular momentum and relative angular momentum by meridional circulations and from the transport of relative angular momentum by small-scale vertical eddy diffusion. The remaining two terms of Eq. (54) represent the exchange of relative angular momentum between the earth's surface and the lower half of the model atmosphere by surface and mountain torques, respectively. According to the computed results, the transport of relative angular momentum by small-scale lateral eddy diffusion and that by large-scale eddies in the lower layer play a minor role in the angular momentum balance.

Fig. 21 displays the 30-day mean latitudinal distribution of the rate of the change of zonal mean relative angular momentum due to various components of the angular momentum balance for the latter half period of 101-130 days. In all figures concerning angular momentum, the values of angular momentum are divided by $a \cdot \cos \phi$. The convergence of relative angular momentum due to the large-scale eddies in the upper layer is shown in the upper part of the same figure. In the middle part of the figure, the transports of relative angular momentum from the lower to the upper layer due to meridional circulations and small-scale vertical eddy diffusion are indicated by solid and dashed lines, respectively. In the lower part, the generation of relative angular momentum by surface and mountain torques is shown by solid and dashed lines, respectively. The scales of the rate of angular momentum change due to the meridional circulation and surface torque are positive upward in the figure, while that due to vertical eddy diffusion and mountain torque is positive downward. Hence, the areas enclosed by solid and dashed lines represent the net rate of the relative angular momentum change caused by the corresponding processes.

In this figure, the January mean convergence of eddy relative angular momentum flux obtained by Tomatsu (1968), the winter mean generation of relative angular momentum due to surface torque obtained by Priestley (1951), and that due to mountain torque (White, 1949) are also plotted by cross, triangle and square symbols. Although the calculated region of the convergence of relative angular momentum is somewhat more southward than that of the actual atmosphere, its magnitude coincides well with the observed. There is a considerable discrepancy between the observed source and sink of angular momentum due to surface and mountain torques and those of the model atmosphere. With respect to the tendency of latitudinal distributions and the regions of the net generation and dissipation due to both effects, however, the calculated results are in agreement with observation.

According to this figure, the surface torque acts to create the zonal mean relative angular momentum in low and high latitudes where surface easterlies prevail, as shown in Fig. 15, while destroying it in the region of surface westerlies. On the other hand, the mountain torque dissipates angular momentum in middle and subtropical latitudes where westerlies

prevail at the 800 -mb level (the flows of this level are assumed to produce the mountain torque), and creates it in high latitudes occupied by easterlies at the 800 -mb level. On the hemispheric mean, although the atmosphere is supplied angular momentum through surface torque, momentum excess is compensated for by the dissipation due to mountain torque. The net effect of both surface and mountain torques yields a source of relative angular momentum in high and low latitudes, and a sink in middle latitudes.

From the middle and upper parts of Fig. 21, we can see that the accumulated angular momentum in the lower layer of high and low latitudes is transferred to the upper layer through the direct meridional circulation existing there, and then is gathered into middle latitudes by the large-scale eddies. The jet stream, the latitude of which is indicated by a circle enclosing the letter J in the figure, exists in this region of convergence of angular momentum. The relative angular momentum converged in middle latitudes is transported downward by the indirect middle latitude cell and counter-balances the sink of angular momentum resulting from the surface and mountain torques. The mechanism of balance of relative angular momentum mentioned above is the same as that obtained by Widger (1949) and Lorenz (1951) from observed data, and obtained by other numerical experiments of the general circulation [see, for example, Smagorinsky, Manabe and Holloway (1965)].

Fig. 22 shows the same as Fig. 21, but for the period of 71-100 days during which the double jet structure is predominant. In comparing Fig. 22 with Fig. 21, the mechanisms of angular momentum balance for both periods turn out to be essentially different from each other in high latitudes. According to Fig. 22, for the first half period, high latitudes are occupied by a sink of relative angular momentum as a result of destruction of it due to both surface and mountain torques as expected from the fact that the west winds prevail in the lower layer of high latitudes as seen in the upper part of Fig. 15. The dissipation of angular momentum in this sink region is compensated by the downward transport of angular momentum due to an indirect polar cell, forming a 4-cell meridional circulation for this period. The lack of angular momentum thus caused in the upper layer of the polar region is counterbalanced by the poleward transport of angular momentum by large-scale eddies. The convergence of this angular momentum transported into high latitudes contributes to the occurrence and development of the north branch of the double jet stream.

In the left and right parts of Fig. 23, the 30-day mean latitudinal distributions of the zonally averaged rate of relative angular momentum change due to each disturbance of wave numbers 1 through 8 are shown for the periods of 71-100 days and 101-130 days, respectively. It can be seen in this figure that the disturbance of wave number 2 plays an important role in the poleward transport of relative angular momentum as well as in the poleward transport of heat indicated in Fig. 20.

8. Energy Balance

Taking the hemispheric mean of Eqs. (41), (42) and (43) multiplied by $-\psi_1$, $-\psi_3$, and $\frac{1}{\sigma}(\frac{R}{p_2})^2 T_2$, respectively, we can derive the energy equations. If these equations are arranged in consideration of Eq. (17) and the following relations

$$\nabla^2\phi_\ell = \nabla(f\nabla\psi_\ell) \qquad (\ell=1, 2, 3) \qquad [\text{from (4)}]$$

$$\alpha_2 = \frac{1}{\Delta p}(\Phi_1-\Phi_3) \qquad (\text{hydrostatic equation})$$

$$\omega_2 = \nabla^2 X_2 \qquad [\text{from (6)}]$$

then the energy equations may be written as follows:

$$\frac{\partial K_1}{\partial t} = \overline{\psi_1 J(\psi_1, \nabla^2\psi_1+f)} - \frac{1}{\Delta p}\overline{\omega_2\Phi_2} - \frac{1}{2}\overline{\omega_2\alpha_2} - A\overline{[(\nabla^2\psi_1)^2 - \frac{2}{a^2}(\nabla\psi_1)^2]}$$

$$+ \frac{g}{\Delta p}\overline{\psi_2\tau_2} - \frac{1}{2}k_i\overline{[\nabla(\psi_1-\psi_3)]^2} \qquad (55)$$

$$\frac{\partial K_3}{\partial t} = \overline{\psi_3 J(\psi_3, \nabla^2\psi_3+f)} + \frac{1}{\Delta p}\overline{\omega_2\Phi_2} - \frac{1}{2}\overline{\omega_2\alpha_2} - A\overline{[(\nabla^2\psi_3)^2 - \frac{2}{a^2}(\nabla\psi_3)^2]}$$

$$- \frac{g}{\Delta p}\overline{\psi_2\tau_2} - \frac{1}{2}k_i\overline{[\nabla(\psi_1-\psi_3)]^2} + \gamma_m\overline{\psi_3 J(h,\psi_3)} + k_s\overline{\psi_3\nabla^2\psi_4} \qquad (56)$$

$$\frac{\partial A}{\partial t} = -\frac{1}{\sigma}\left(\frac{R}{p_2}\right)^2\overline{\overline{T_2 J(\psi_2, T_2)}} + \overline{\overline{\omega_2\alpha_2}} - A\overline{\overline{(\nabla T_2)^2}} + \frac{g}{2C_p\Delta p}\overline{\overline{T_2''Q''}} \qquad (57)$$

where K_1, K_3, A and α are the kinetic energy per unit mass in the upper layer, that in the lower layer, the available potential energy per unit mass and the specific volume of air, respectively, and $\overline{\overline{(\ )}}$ and $(\ )''$ denote the area mean over the hemisphere and the deviation from its area mean, i.e.,

$$\overline{\overline{(\ )}} = \frac{1}{4\pi a^2}\int_0^{2\pi}\int_{-\frac{\pi}{2}}^{\frac{\pi}{2}}(\ )\, a^2 \cos\phi\, d\phi d\lambda$$

$$(\ )'' = (\ ) - \overline{\overline{(\ )}}$$

Although the first terms in (55) and (56) vanish, these terms contribute to the redistribution of kinetic energy in each layer between the zonal motion and disturbances and among the disturbances. The second and fifth terms represent the exchange of kinetic energy between the upper and lower layers through the pressure force and the stress by vertical eddy diffusion, respectively. The third, fourth and sixth terms are the rate of conversion of available potential energy into kinetic energy, the rate of dissipation of kinetic energy due to lateral eddy diffusion and that due to vertical eddy diffusion, respectively. In (56), the seventh term, which contributes to the redistribution of kinetic energy between the zonal motion and the disturbances and among the disturbances through the deformation of flow due to mountains, is equal to zero. This is consistent with the fact that the deformation of flow due to mountains causes no change of total energy. The last term in (56) represents the dissipation of kinetic energy due to surface friction. In (57), the first term, which is equal to zero, contributes to the redistributions between the zonal and eddy available potential energy and among the available potential energy of various disturbances. In the same equation, the second, third and fourth terms represent the conversion between available potential energy and kinetic energy, the dissipation of available potential energy due to lateral eddy diffusion and the generation of this energy due to diabatic heating. In the energy Eqs. (55) and (56), the equal partition of the conversion of

potential energy into kinetic energy and that of the dissipation of kinetic energy due to vertical eddy diffusion into the upper and lower layers result from the fact that Φ_2 and ψ_2 in the terms $\frac{1}{\Delta p}\omega_2\Phi_2$ and $\frac{g}{\Delta p}\psi_2\tau_2$ measured at the 600 -mb level are assumed to be equal to the average of the values of the upper and lower levels of the corresponding quantities.

In the upper and lower parts of Fig. 24, the 30-day mean energy diagrams are shown for the air column of unit mass for the first and latter half periods, respectively. In each part, K_Z and K_E in the upper and lower boxes represent the hemispheric mean of zonal and eddy kinetic energy in the upper and lower layers, respectively. A_Z and A_E are the hemispheric mean of zonal and eddy available potential energy. The notations Q, H.D., I.F. and S.F. in the boxes denote the change of available potential energy due to diabatic heating and the destructions of energy due to lateral eddy diffusion, to vertical eddy diffusion and to surface friction, respectively. ADV. MT., I.F., and L.S.E., near the arrows indicating the direction of energy transformation, represent the transformation of kinetic energy due to the effect of the advection term, that due to the effect of mountains, the transport of energy due to vertical eddy diffusion and that due to the pressure force, respectively.

From this figure, with regard to the main sources and sinks of the various energy components, the following facts may be found:

1. The zonal available potential energy is created by diabatic heating and transferred to eddy available potential energy. In spite of a smaller pole to equator temperature gradient for the first half period relative to the latter half period, the larger value for the generation of zonal available potential energy by diabatic heating for the first half period means that the warming in the equatorial region and the cooling in the polar region is stronger for this period, characterized by the appearance of the predominant double jet structure.

2. The eddy available potential energy transformed from zonal available potential energy is converted to eddy kinetic energy.

3. The eddy kinetic energy in the upper layer, fed by the conversion of potential energy and the transport of energy from the lower layer through the pressure force, dissipates by transformation into zonal kinetic energy and by the effects of vertical and horizontal eddy diffusion. The magnitude of these three effects of dissipation are almost the same.

4. The lower layer is supplied eddy kinetic energy by baroclinic effects and transformation of zonal kinetic energy through the influence of mountains. This energy is lost by surface friction and transport to the upper layer through pressure forces.

5. In the upper layer, zonal kinetic energy transformed from eddy kinetic energy dissipates mainly by the effect of vertical eddy diffusion.

6. The zonal kinetic energy in the lower layer is fed by the conversion of potential energy and the net effect of vertical eddy diffusion. (Since the magnitude of energy transport from the upper to the lower layer through the vertical eddy stress is quite large, the net effect of the transport and the dissipation due to vertical eddy diffusion is to increase the zonal kinetic energy in the lower layer. This is also true in the case of eddy kinetic energy.) The main sink of this energy is the transformation into eddy kinetic energy through the effect of mountains.

According to the comparison between the upper and lower parts of the same figure, the transformation of energy from A_Z to A_E and from A_E to K_E is larger in the first half period than in the latter half period, although the pole to equator temperature gradient is smaller in the first half period, as was pointed out before. The non-adiabatic heating acts to dissipate eddy available potential energy for the first half period, while creating it during the latter half period. The reason for the differences described above will be made clear by the following spectral consideration of energy transformation. For the latter half period, the effect of surface friction acts to produce zonal kinetic energy in the lower layer, although the amount of its production is quite small. This deficiency of our model results from the linear extrapolation of surface wind from the winds of the 400- and 800 -mb levels. For the first half period, the transport of zonal kinetic energy through the pressure force is from the upper to the lower layer. This is consistent with the fact that the effect of the indirect meridional circulation becomes prevalent because of the formation of a 4-cell meridional circulation during this period. It is of interest that the zonal kinetic energy in the lower layer is larger for the first half period than for the latter half period in spite of a smaller value of the zonal kinetic energy in the upper layer for the first half period.

For comparison, our results for the various components of energy and energy transformations for the latter half period are shown with the

observed results compiled by Oot (1964) and the results obtained from other numerical experiments [i.e., Smagorinsky, Manabe, Holloway (1965), Smagorinsky (1963), and Phillips (1956)] in Table I. In this table, the notation (A_Z, A_E) represents the transformation of energy from A_Z to A_E and the other notations are interpreted in the same manner. D_S means the dissipation of energy.

In the upper and lower parts on the left-hand side of Fig. 25, 30-day mean spectral distributions of kinetic energy of the upper and lower layers in the air column of unit mass are shown respectively. The right part of the figure shows the 30-day mean spectral distribution of available potential energy in the air column of unit mass. In this figure, the solid lines indicate the distribution for the first half period, while the dashed lines indicate the distribution for the latter half period. The corresponding winter mean values obtained by Saltzman and Fleisher (1961; 1962) are plotted by solid circles. From Fig. 25, it is found that the disturbance of wave number 2, which plays an important role in the transport of heat and angular momentum for the period characterized by the predominant double jet structure, has larger energy for this period than for the latter half period. Thus, it turns out that the disturbance of wave number 2 appears to be very significant in the blocking situation appearing for the first half period. According to comparison with observation, the calculated available potential energy is considerably smaller than the observed values at wave numbers 1 and 2.

Fig. 26 shows the 30-day mean spectral distributions for various components of energy transformations in the air column of unit mass. The notation used in this figure will be interpreted with ease from the explanations in the preceding figures and the table. Here K_{up} and K_{Lw} stand for kinetic energy in the upper and lower layers, and (A_E, A_E)or(K_E, K_E) means the energy transformation amongst the disturbances.

From parts (A), (C) and (D) of this figure, we find that, as expected from baroclinic instability theory, the transformation from zonal to eddy available potential energy, the conversion from available potential energy to kinetic energy and the energy transfer from the lower to the upper layer indicates large values around wave number 5 (the static stability adopted in our model is such that maximum instability occurs at wave number 5).

On the other hand, each distribution of these energy transformations indicates a maximum at wave number 2 for the first half period. The growth of the disturbance of wave number 2, significant in the blocking situation, results mainly from this instability which is inexplicable by the so-called baroclinic instability theory. A key point to clarifying the blocking mechanism would be an explanation of growth in this wave number. In connection with this, it is of special interest that, as seen in part (G) of the figure, the distribution of transformation for zonal to eddy kinetic energy through the effect of mountains indicates a maximum value at wave number 2 for the first half period, in contrast to its disappearance for the latter half period. Part (E) shows that almost all disturbances dissipate their kinetic energy to feed the zonal motion.

From part (I) of the same figure, we can see that the available potential energy of the disturbances around wave number 2 is created by the diabatic heating for both periods. This would result from higher temperature and stronger heating over the oceans than over the continents. The larger available potential energy of the disturbance of wave number 2 for the first half period, as indicated in Fig. 25, means that the atmospheric temperature is higher over the oceans and lower over the continents for the first half period than for the latter half period. However, since the increase of atmospheric temperature increases the cooling of the atmosphere due to long wave radiation and suppresses the transport of heat from the earth's surface to the atmosphere over the oceans, it results in decreasing the heating of the atmosphere. For the reverse reason, the decrease of atmospheric temperature increases the heating of the atmosphere. Thus, it would be inferred that the decrease of generation of available potential energy of wave number 2 by non-adiabatic heating for the first half period is due to the fact that the heating of the atmosphere decreases over the oceans and increases over the continents for this period, characterized by the predominant double jet structure.

Fig. 27 is prepared to examine the kinetic energy balance of the disturbance of wave number 2 in more detail. In the upper and lower parts of this figure, the budgets of kinetic energy in the upper and lower layers, respectively, are shown. In each part, the two left columns indicate the gain and loss of kinetic energy for the first half period, while the two right columns describe the latter half period. The notation written in

the columns represents the processes through which the disturbance of wave number 2 obtains or dissipates energy. The notation BC means the net effect of the conversion of potential energy and the transfer of kinetic energy from the lower layer through the pressure force, and BT denotes the net effect of exchange of kinetic energy between the disturbance of wave number 2 and the zonal motion and between that and the other disturbances through the advective term. The other notation was already explained in the preceding figures. According to this figure, it is found that, in the upper layer, the disturbance of wave number 2 is supplied energy due to the conversion of potential energy and the transport of kinetic energy from the lower, while in the lower layer it is supplied energy mainly by the transformation of zonal kinetic energy through the deformation of zonal flow caused by mountains. The difference between the energy budgets of the two periods is that, in the lower layer, the process represented by BT acts as an energy source and the process represented by BC acts as an energy sink (this means that the transport of energy into the upper layer is larger than the conversion of available potential energy into the lower layer) for the first half period; the reverse is true for the latter half period. This feature of the computed results in the predominant blocking situation is in qualitative agreement with the observed energy budget of the significant wave in the blocking action of January 1963 as obtained by Murakami and Tomatsu (1965). In the upper layer, the large amount of kinetic energy of this disturbance converted from available potential energy by the baroclinic effect is lost to maintain the zonal motion. This would mean that the blocking phenomenon should not be considered as a barotropic process, but as a baroclinic process.

9. Summary

Through a time integration of the geostrophic system of equations, including both effects of orography and heating contrast due to land-sea distribution, a blocking process very similar to that observed in the actual atmosphere was produced.

For the period during which the predominant double jet structure (resulting from the occurrence of active blocking) appears in the latitudinal distribution of the zonally averaged zonal wind, the unusual

poleward transport of heat by large-scale eddies causes warming of the polar region accompanied by the formation of an indirect meridional circulation, as seen from the analyzed computations. In the upper layer at high latitudes, the angular momentum is transported poleward by large-scale eddies to compensate for the destruction of angular momentum due to this indirect cell. The convergence of this angular momentum transported into high latitudes controls the formation and development of the north branch of the double jet stream.

The poleward transport of heat and angular momentum which plays an important role in the initiation and maintenance of the double jet stream, is performed primarily by the disturbance of wave number 2 which shows a large growth for this period.

In the upper layer this disturbance, being significant in the active blocking situation, is fed by the conversion of available potential energy and the transfer of kinetic energy from the lower layer. The zonal motion is maintained by the energy supply from this disturbance. In the lower layer, when this disturbance is developing well, its main energy source is the transformation from the zonal kinetic energy through the effect of topography. This seems to indicate that the effect of mountains is one of the factors causing the growth of the disturbance of wave number 2. In order to clarify the mechanism of the blocking process, the development of a new instability theory which can explain the growth of this kind of disturbance is desirable.

On the other hand, the effects of diabatic heating are summarized as follows:

1. The meridional gradient of diabatic heating is larger during the period characterized by active blocking, while
2. the difference of diabatic heating between the ocean and the continent is smaller.

In this study some characteristic properties concerning blocking and double jet structure -- reproduced by our relatively simple model atmosphere -- are determined, and these should be verified by observations in the actual atmosphere. Thus, further studies of the budgets of heat, angular momentum and energy during the period of a blocking situation are needed.

ACKNOWLEDGMENTS

The greater part of this work was done at the Meteorological Research Institute of Japan and completed at Colorado State University through the support of the National Science Foundation.

The author is deeply grateful to Dr. F. Baer for valuable comments, encouragements and reviewing the original manuscript. He wishes also to express his thanks to Dr. K. Takahashi, Dr. S. Kubota and the staff members of the forecasting laboratory of M.R.I. for many stimulating discussions.

The help of Mrs. Y. Honda, Messrs. E. Yajima and N. Uchiyama in preparing the figures, and Mrs. P. Stollar in typing the manuscript is appreciated.

REFERENCES

Adem, J., 1962: On the theory of the general circulation. Tellus, 14, 102-115.

Adem, J., 1964: On the physical basis for the numerical prediction of monthly and seasonal temperatures in the troposphere ocean continent. Mon. Wea. Rev. 92, 91-103.

Asakura, T. and A. Katayama, 1964: On the normal distribution of heat sources and sinks in the lower troposphere over the northern hemisphere. J. Met. Soc. Japan, Ser. II, 42, 209-244.

Baer, F. and G.W. Platzman, 1961: A procedure for numerical integration of the spectral vorticity equation. J. Meteor., 18, 393-401.

Baer, F., 1964: Integration with the spectral vorticity equation. J. Atmos. Sci., 21, 260-276.

Berggren, R., B. Bolin and C-G. Rossby, 1949: An aerological study of zonal motion, its perturbations and break-down. Tellus, 1, 14-37.

Berry, F.A., W.H. Haggard and P.M. Wolff, 1954: Description of contour patterns at 500 millibars. Project AROWA, BU of AERO. (TED-UNL-MA-501), Norfolk, Virginia.

Burdecki, F., 1955: A study of temperature distribution in the atmosphere. Notos, 4, 192-203.

Burger, A.P., 1958: Scale consideration of planetary motions of the atmosphere. Tellus, 10, 195-205.

Charney, J.G., 1959: On the theory of the general circulation of the atmosphere. The Atmosphere and the Sea in Motion. New York, The Rockefeller Institute Press, 135-162.

Deland, R.J., 1965: On the scale analysis of traveling planetary waves. Tellus, 17, 527-528.

Elliot, P.D. and T.B. Smith, 1949: A study of effects of large blocking high on the general circulation of the northern hemisphere westerlies. J. Meteor., 6, 67-85.

Garriott, E.B., 1904: Long range forecasts. U.S. Weather Bureau Bulletin, No. 35, Wash. D.C.

Kasahara, A. and W.M. Washington, 1967: NCAR global general circulation model of the atmosphere. Mon. Wea. Rev., 95, 389-402.

Lorenz, E.N., 1951: Computations of the balance of angular momentum and the poleward transport of heat. Sci. Rep. No. 6, M.I.T. Gen. Circ. Proj., Contract No. AF19(122)-53.

Lorenz, E.N., 1960: Energy and numerical weather prediction. Tellus, 12, 364-373.

Manabe, S., J. Smagorinsky and R.F. Strickler, 1965: Simulated climatology of a general circulation model with a hydrologic cycle. Mon. Wea. Rev., 93, 769-798.

Mintz, Y.A., 1954: The observed zonal circulation of the atmosphere. Bull. Amer. Meteor. Soc., 35, 208-214.

Mintz, Y.A. and J. Lang, 1955: A model of the mean meridional circulation. Final Report, Article 6, Contract AF19(122)-48, Department of Meteorology, University of California, Los Angeles.

Mintz, Y., 1964: Very long-term global integration of the primitive equations of atmospheric motion. Proceedings of the WMO/IUGG Symposium on the Research and Development Aspects of Long-Range Forecasting, Boulder, Colo., WMO Technical Note, No. 66, 141-167.

Murakami, T. and K. Tomatsu, 1965: Energy cycle in the lower atmosphere. J. Meteor. Soc. Japan, Ser. II, 43, 73-89.

Namias, J., 1947: Characteristic of the general circulation over the northern hemisphere during the abnormal winter 1946-1947. Mon. Wea. Rev., 75, 145-152.

Oort, A.H., 1964: On estimates of the atmospheric energy cycle. Mon. Wea. Rev., 92, 483-493.

Phillips, N.A., 1956: The general circulation of the atmosphere: a numerical experiment. Q.J. Roy. Met. Soc., 82, 123-164.

Platzman, G.W., 1960: The spectral form of the vorticity equation. J. Meteor., 17, 635-644.

Platzman, G.W., 1962: The analytical dynamics of the spectral vorticity equation. J. Atmos. Sci., 19, 313-328.

Priestley, C.H.B., 1951: A survey of the stress between the ocean and atmosphere. Austr. J. Sci. Res., Series A4, 315-328.

Rex, D.P., 1950a: Blocking action in the middle troposphere and its effect upon regional climate. I. An aerological study of blocking. Tellus, 2, 196-211.

Rex, D.P., 1950b: Blocking action in the middle troposphere and its effect upon regional climate. II. The climatology of blocking action. Tellus, 2, 275-301.

Rossby, C-G., 1950: On the dynamics of certain types of blocking waves. J. Chinese Geophys. Soc., 2, 1-13.

Saltzman, B. and A. Fleisher, 1961: Further statistics on the modes of release of available potential energy. J. Geophys. Res., 66, 2271-2273.

Saltzman, B. and A. Fleisher, 1962: Spectral statistics of the wind at 500 mb. J. Atmos. Sci., 19, 195-204.

Saltzman, B. and S. Teweles, 1964: Further statistics on the exchange of kinetic energy between harmonic components of the atmospheric flow. Tellus, 16, 432-435.

Serebreny, S.M., E.J. Wiegman and R.G. Hadfield, 1957: A study of jet stream conditions in the northern hemisphere during winter. Technical Report No. 5, Project AROWA Contract No. N600(188)40835.

Silberman, I., 1954: Planetary waves in the atmosphere. J. Meteor., 11, 27-34.

Smagorinsky, J., 1963: General circulation experiments with the primitive equations: I. The basic experiment. Mon. Wea. Rev., 91, 99-164.

Smagorinsky, J., S. Manabe and J.L. Holloway, 1965: Numerical results from a nine-level general circulation model of the atmosphere. Mon. Wea. Rev., 93, 727-768.

Thompson, P.D., 1957: A heuristic theory of large-scale turbulence and long period velocity variations in barotropic flow. Tellus, 9, 69-91.

Tomatsu, K., 1968: To be published.

White, R.M., 1949: The role of mountains in the angular-momentum balance of the atmosphere. J. Meteor., 6, 353-355.

Widger, W.K., 1949: A study of the flow of angular momentum in the atmosphere. J. Meteor., 6, 291-299.

Wiin-Nielsen, A., J.A. Brown and M. Drake, 1963: On atmospheric energy conversions between the zonal flow and the eddies. Tellus, 15, 261-279.

Yeh, T.C., 1949: On energy dispersion in the atmosphere. J. Meteor., 6, 1-16.

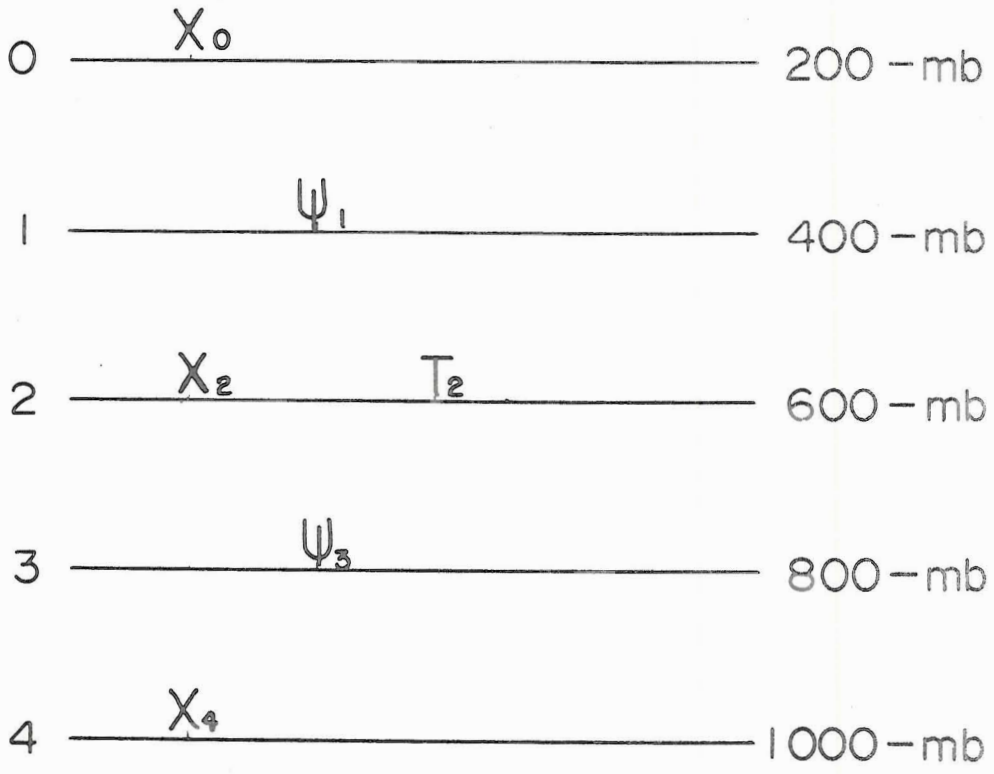

Fig. 1 - Two-layer representation of the model atmosphere; notation indicates levels to which model variables refer.

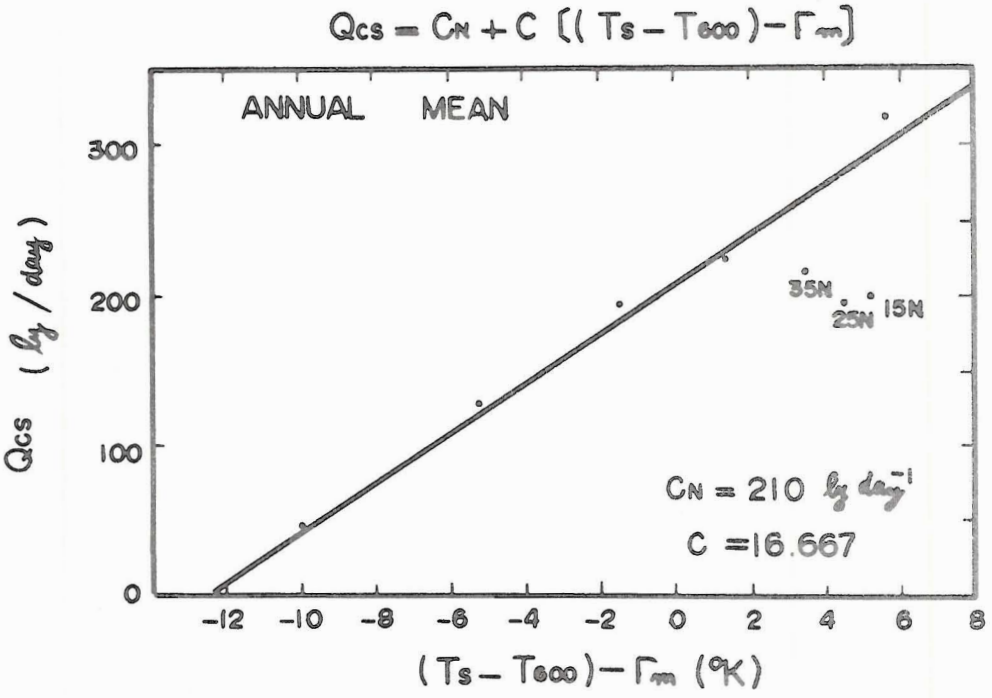

Fig. 2 - The relationship between Q_{CS} and $(T_s - T_{600}) - \Gamma_m$, as employed in model and indicated by solid line. Solid circles indicate zonally averaged annual mean data plotted at 10° latitude intervals starting at 5°N.

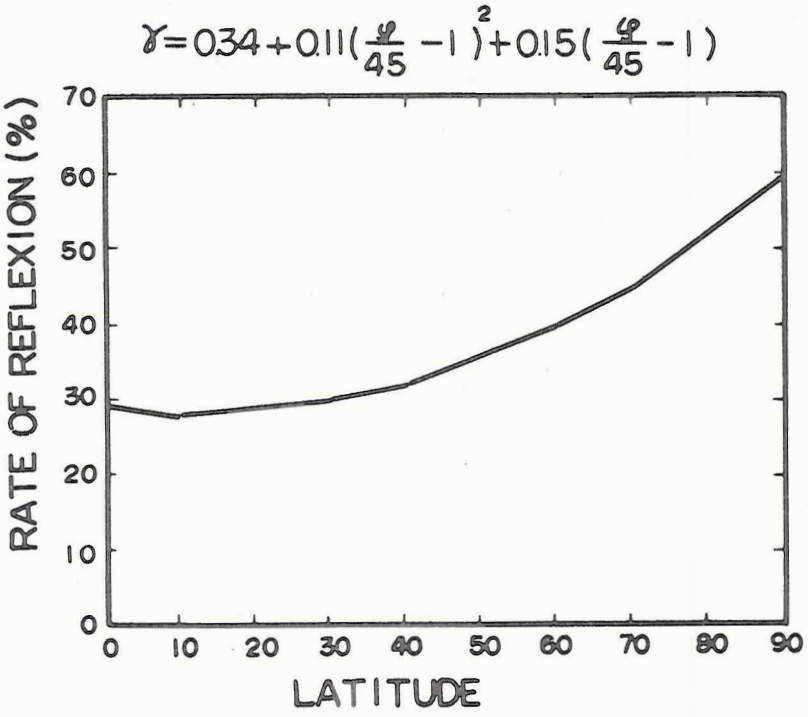

Fig. 3 - Latitudinal distribution of the planetary albedo (%) adopted in the model.

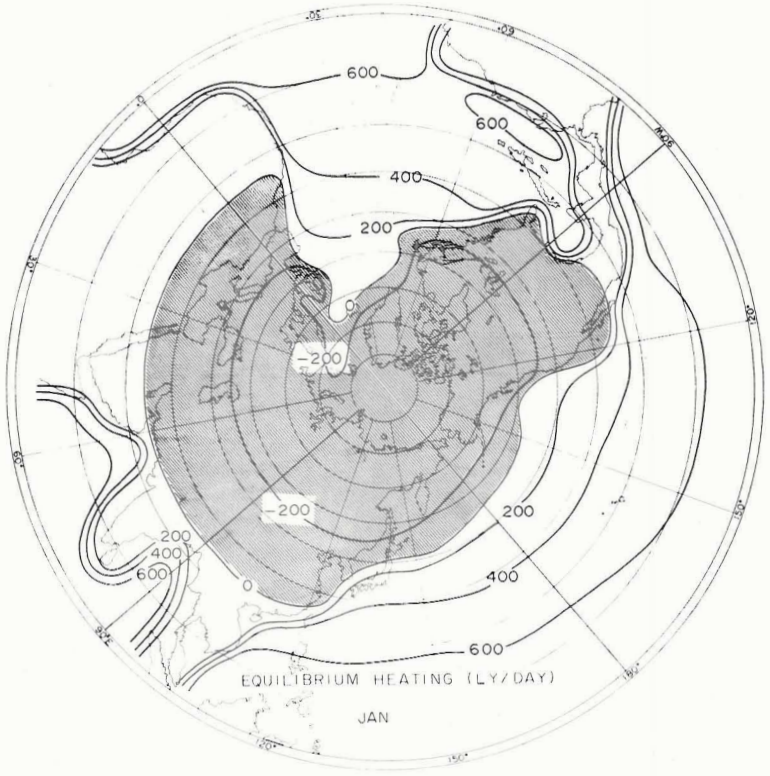

Fig. 4a - Geographical distribution of E (ly/day) in January.

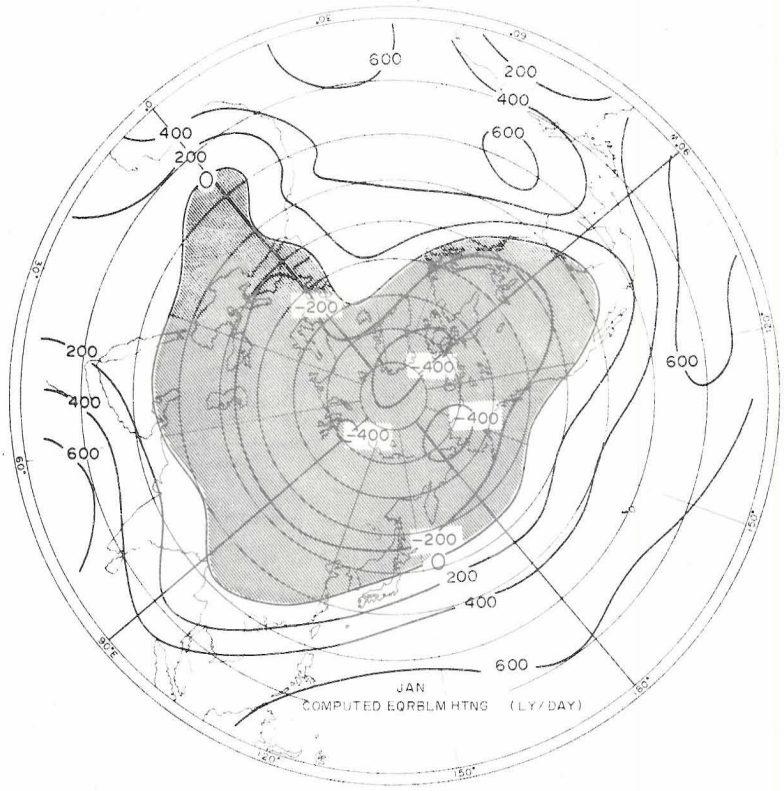

Fig. 4b - Geographical distribution of E (ly/day) adopted in the model, reproduced by using the surface spherical harmonics truncated at $|m| \leq 8$ and $n-|m| \leq 11$, where m and n are the rank and degree of the surface spherical harmonic, respectively.

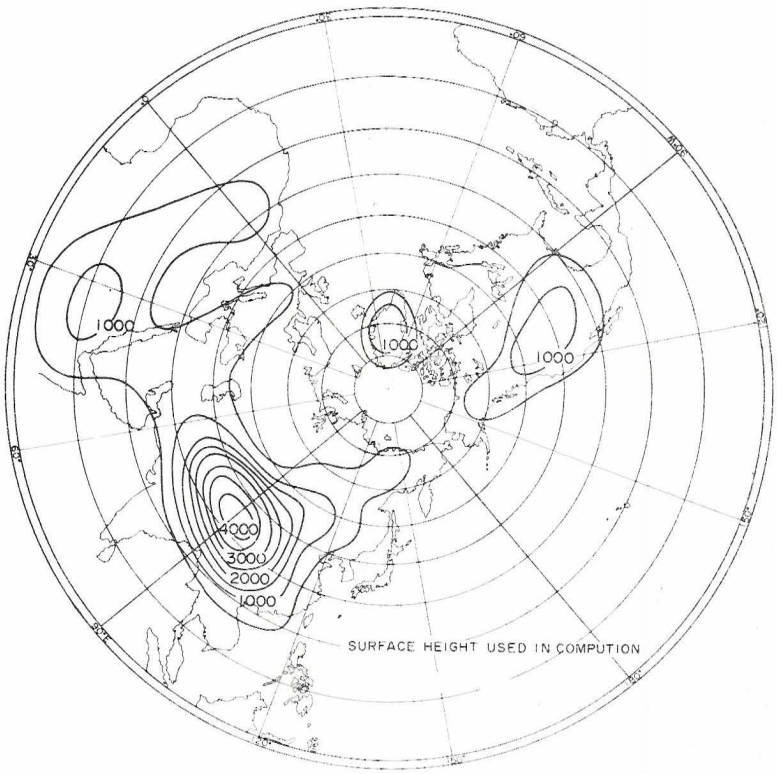

Fig. 5 - Geographical distribution of orographic height (meters) used in the model.

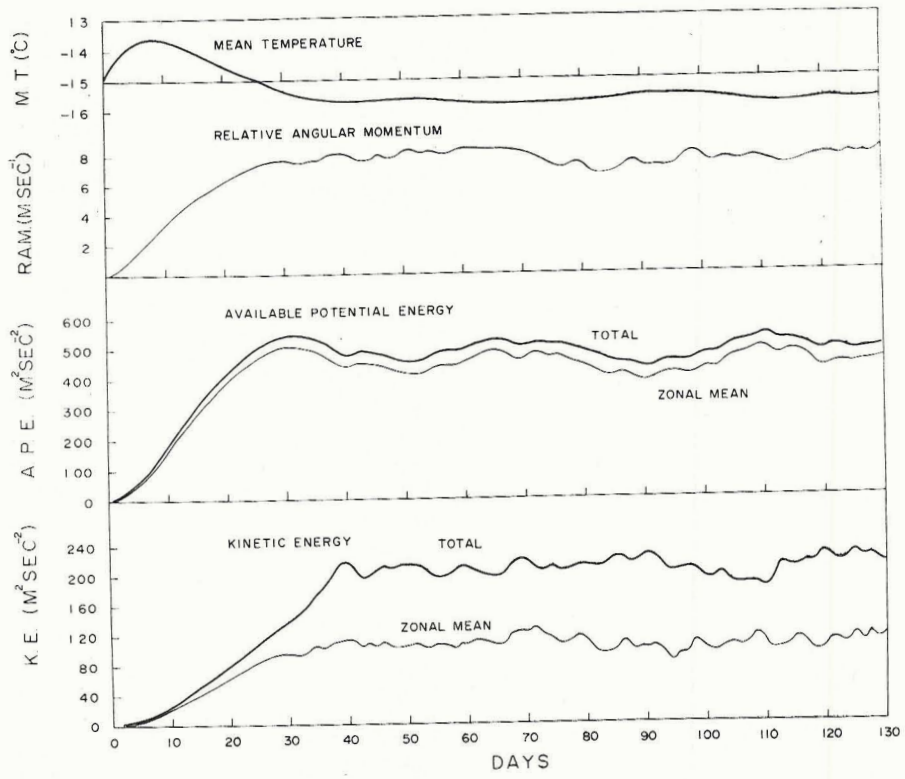

Fig. 6 - Time variations of hemispheric mean temperature (upper part), hemispheric mean of relative angular momentum per unit mass per unit sphere (second part), total and zonal available potential energy per unit mass (third part), and total and zonal kinetic energy per unit mass (lower part).

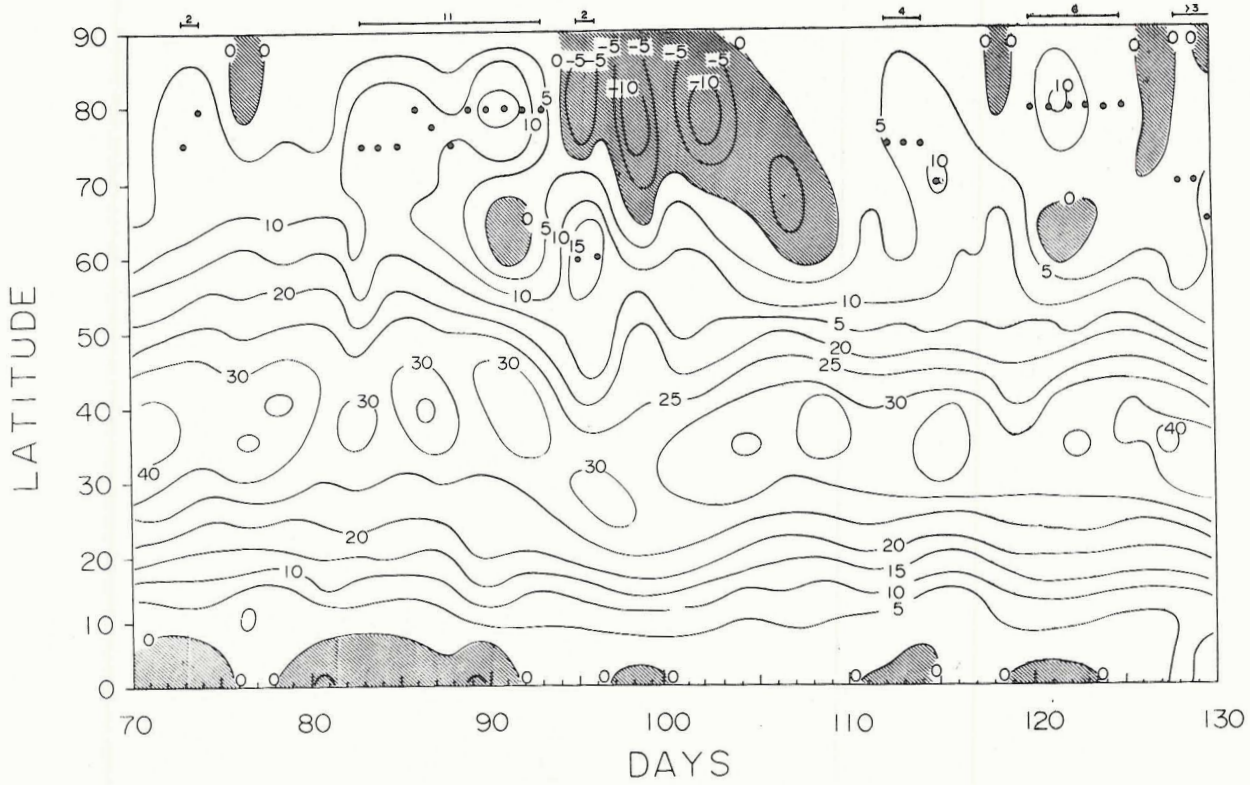

Fig. 7 - Time variation of the latitudinal distribution of the zonally averaged zonal current (m/sec) at the upper level of the model atmosphere. Solid circles indicate the latitude of the secondary wind maximum. Short lines and numbers above the figure indicate the duration of the double jet structure in days, respectively. Shaded areas stand for easterlies.

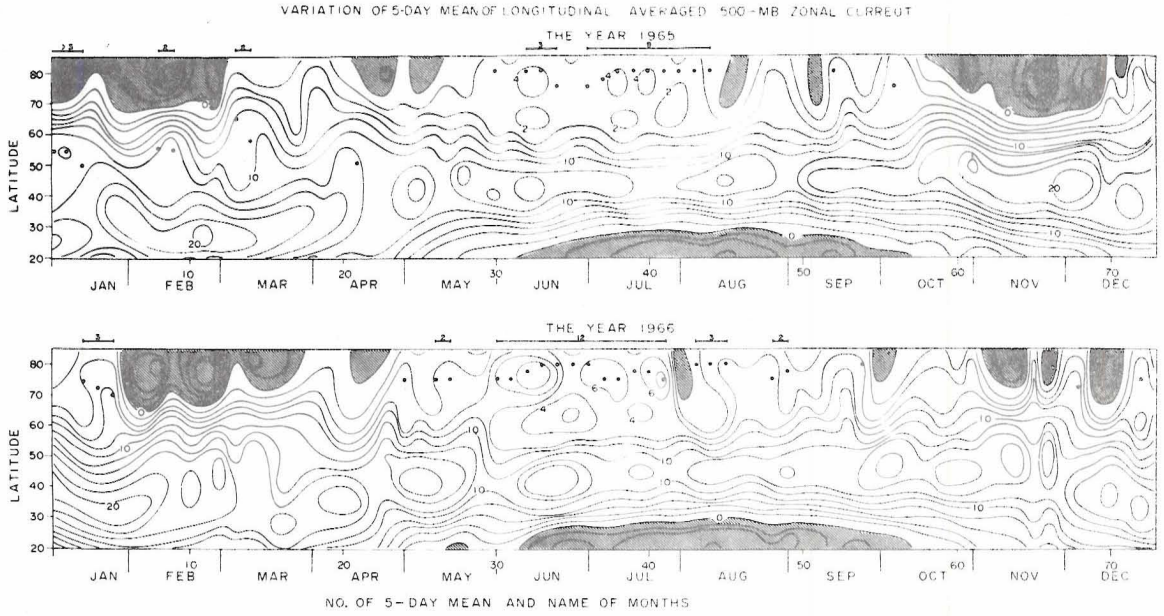

Fig. 8 - Annual variations of the latitudinal distribution of the 5-day mean zonally averaged zonal wind (m/sec) at the 500 -mb level for the years 1965 (upper part) and 1966 (lower part). The numbers attaching short lines above the figure (representing the duration of double jet streams) are in units of 5 days.

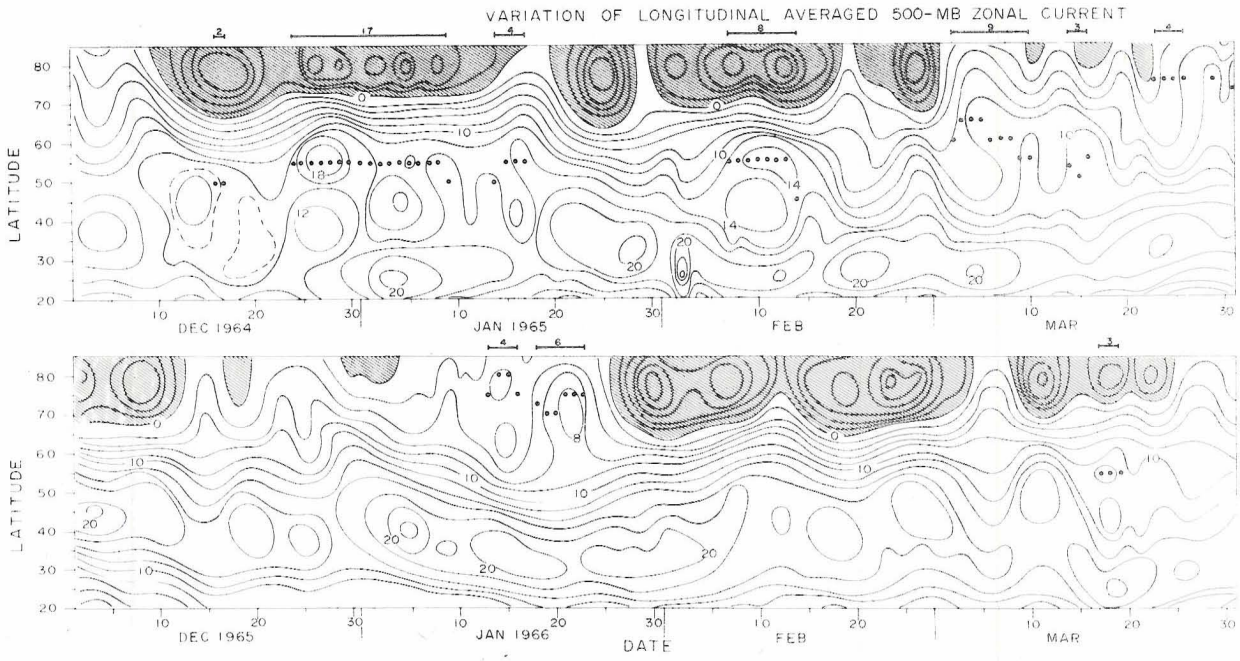

Fig. 9 - Daily variation of the latitudinal distribution of the zonally averaged zonal wind (m/sec) at the 500 -mb level for the periods December 1964 through March 1965 (upper part) and December 1965 through March 1966 (lower part). For further explanations, refer to Fig. 7.

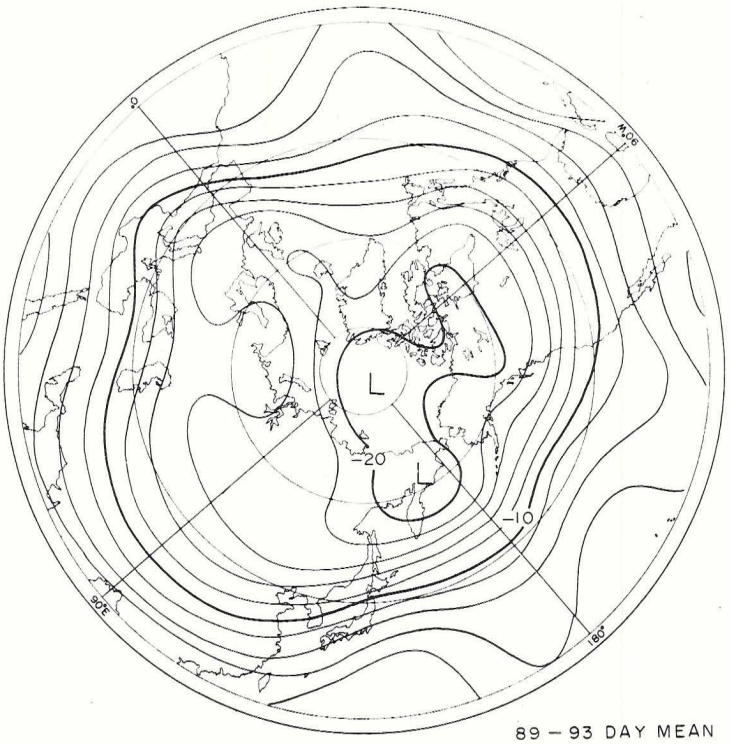

Fig. 10 - 89-93 day mean computed stream lines at the 400 -mb level. (Units: a•m sec^{-1}, where a is the radius of the earth).

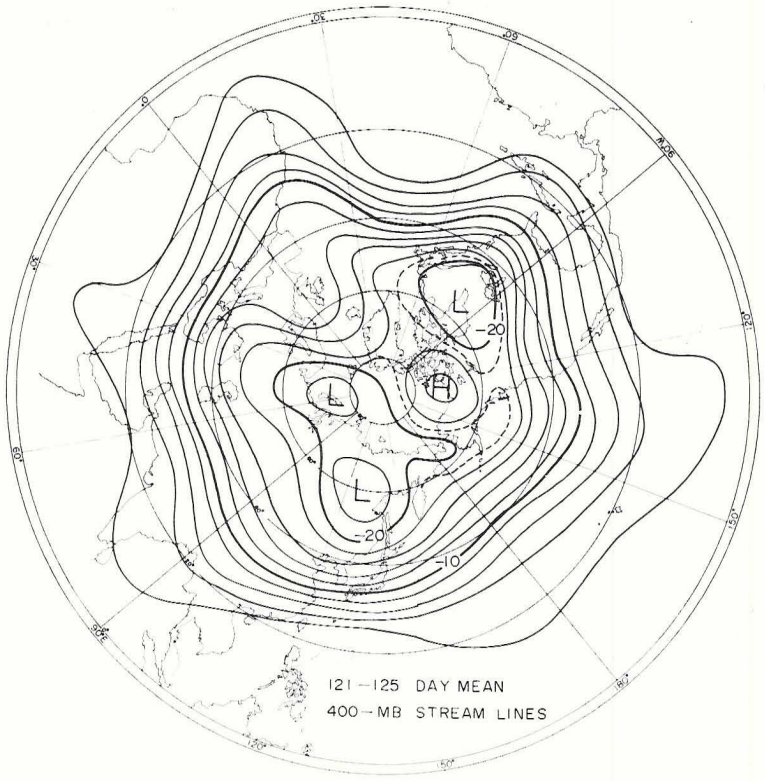

Fig. 11 - 121-125 day mean computed stream lines at the 400 -mb level. (Units: a•m sec^{-1}).

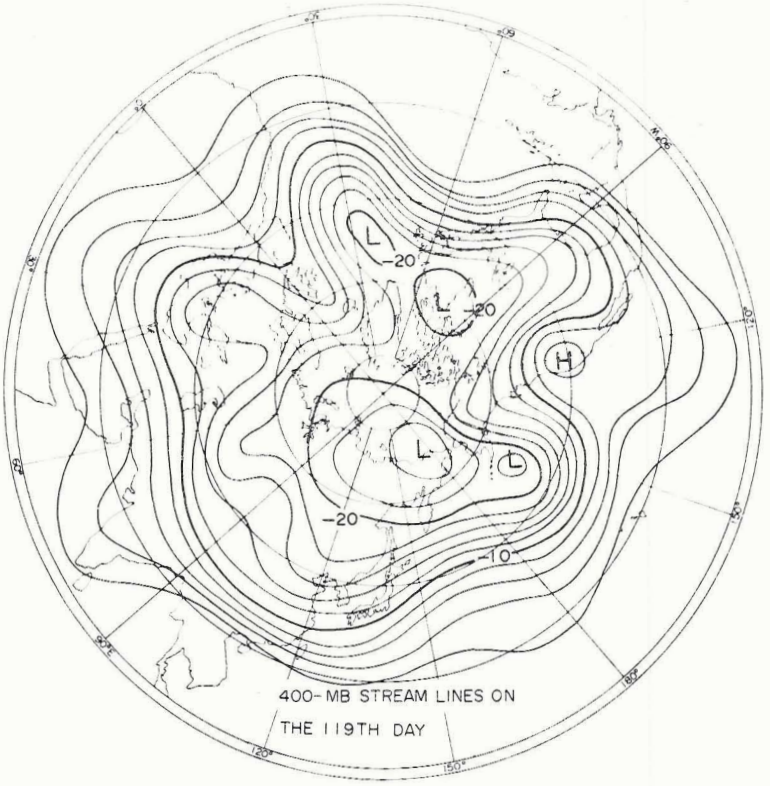

Fig. 12a - 400 -mb stream lines at 119 days. (Units: a.m sec^{-1}).

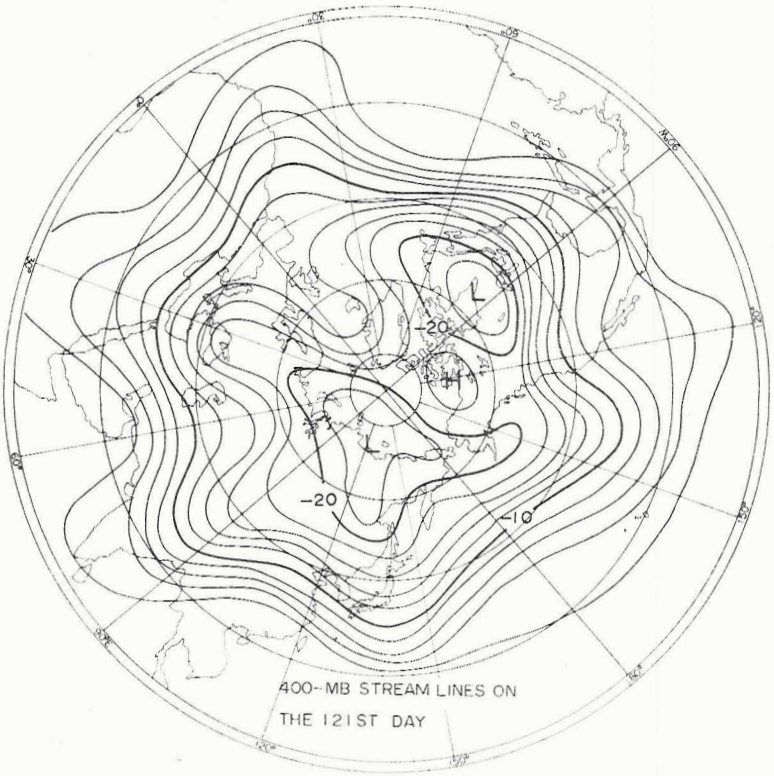

Fig. 12b - 400 -mb stream lines at 121 days. (Units: a.m sec^{-1}).

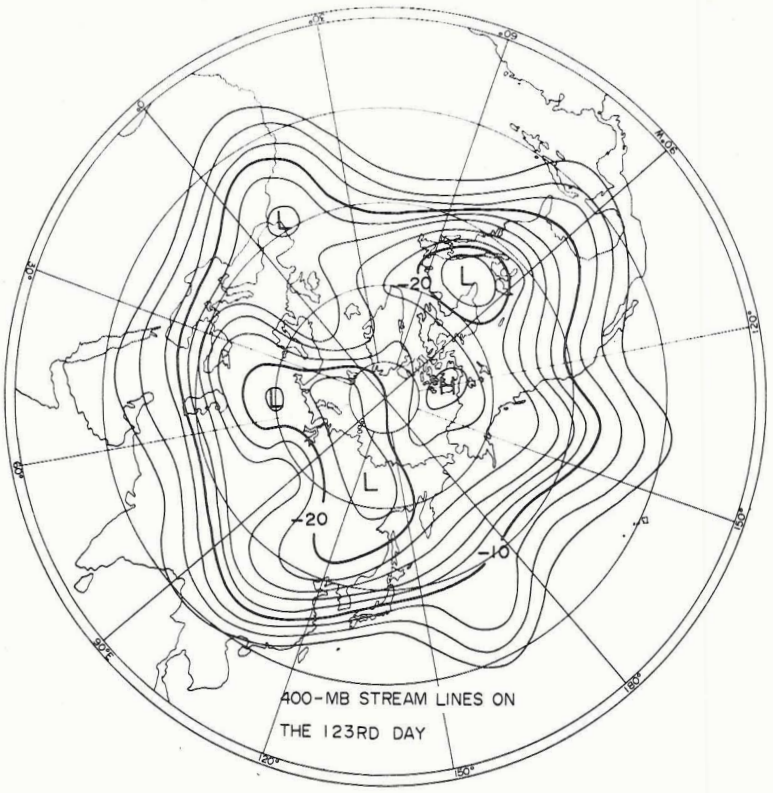

Fig. 12c - 400 -mb stream lines at 123 days. (Units: a.m sec^{-1}).

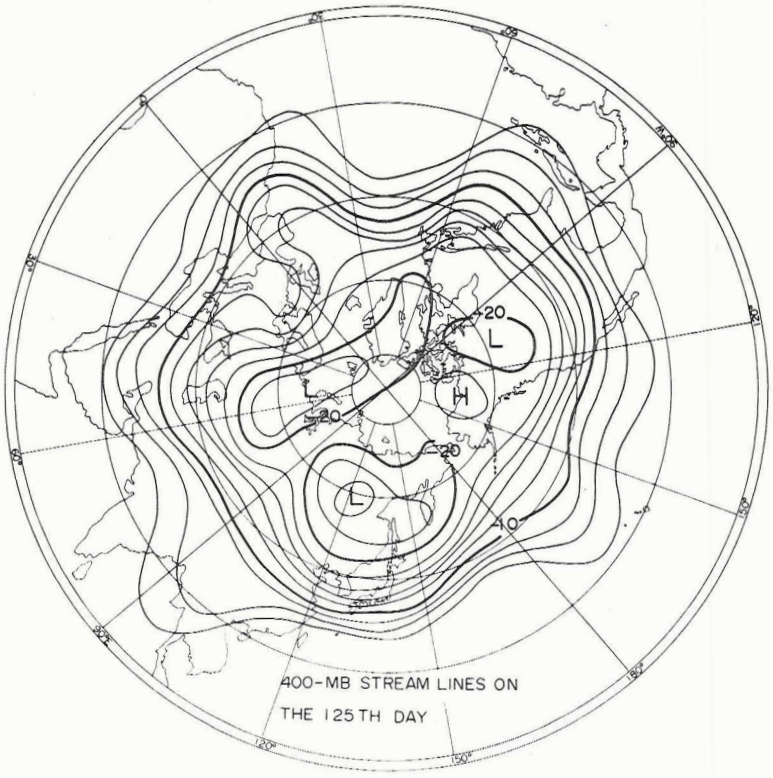

Fig. 12d - 400 -mb stream lines at 125 days. (Units: a.m sec^{-1}).

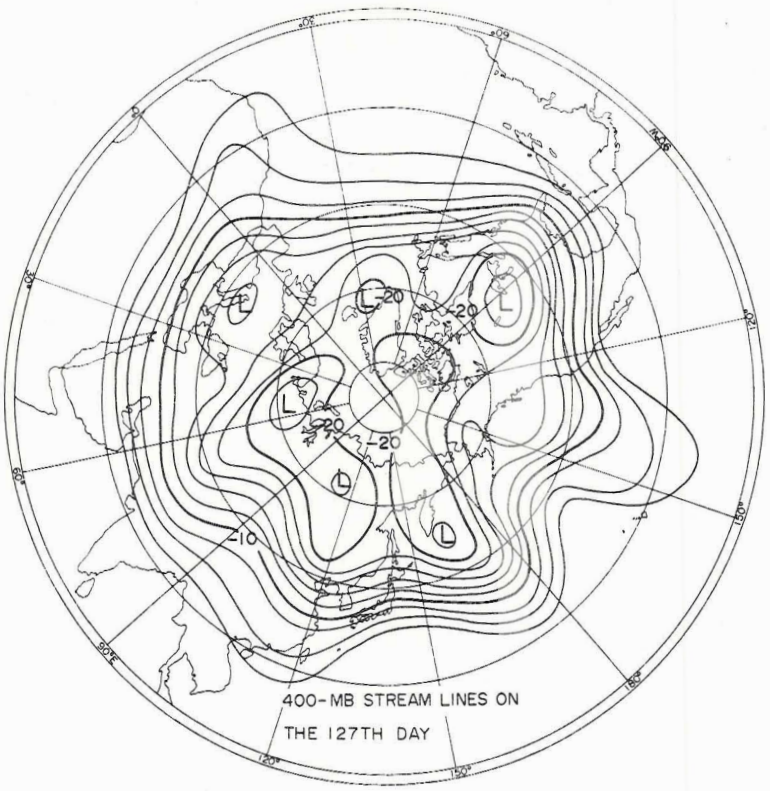

Fig. 12e - 400 -mb stream lines at 127 days. (Units: a.m sec^{-1}).

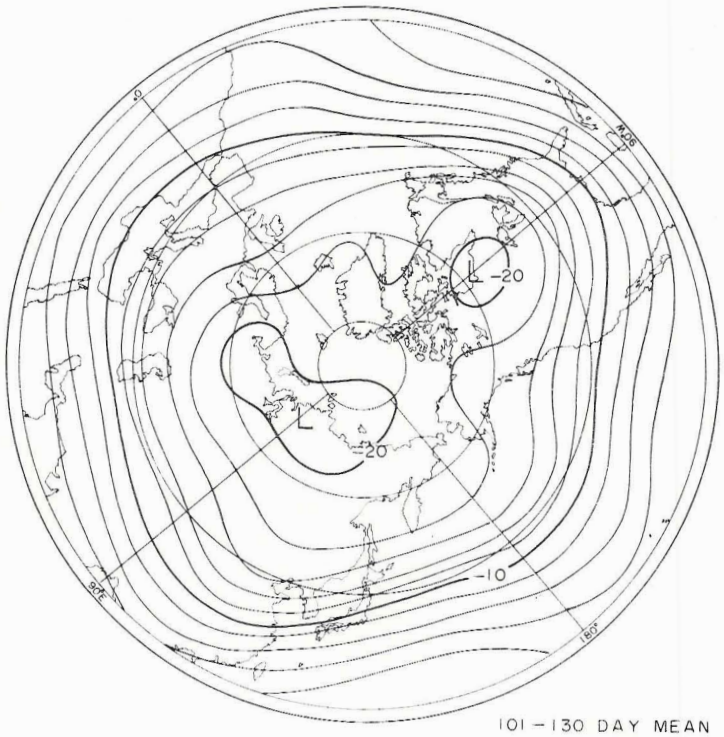

Fig. 13 - 30-day mean computed stream lines (a.m sec^{-1}) at the 400 -mb level for the period of 101-130 days.

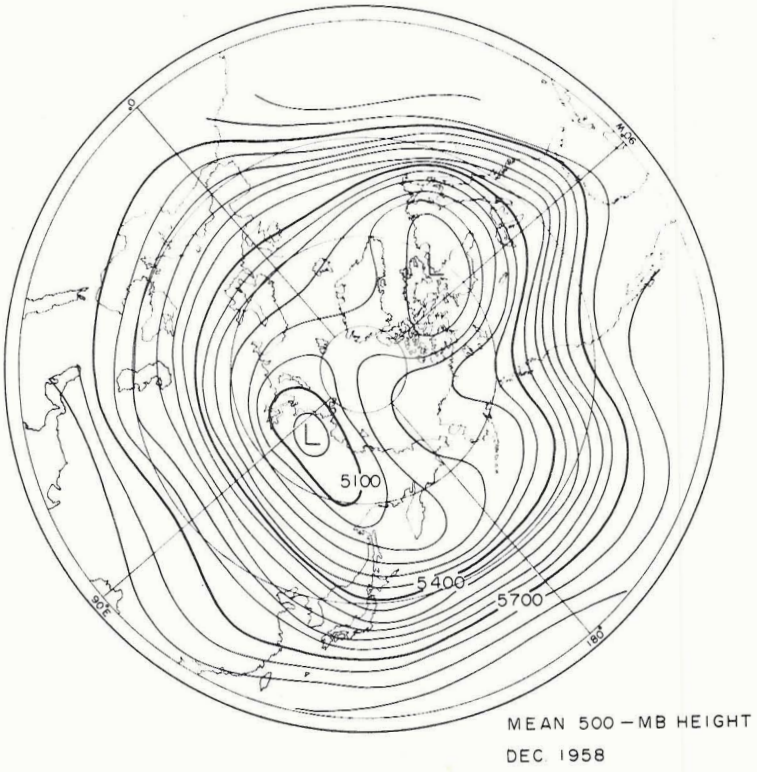

Fig. 14 - 30-day mean 500 -mb contours (meters) for December 1958.

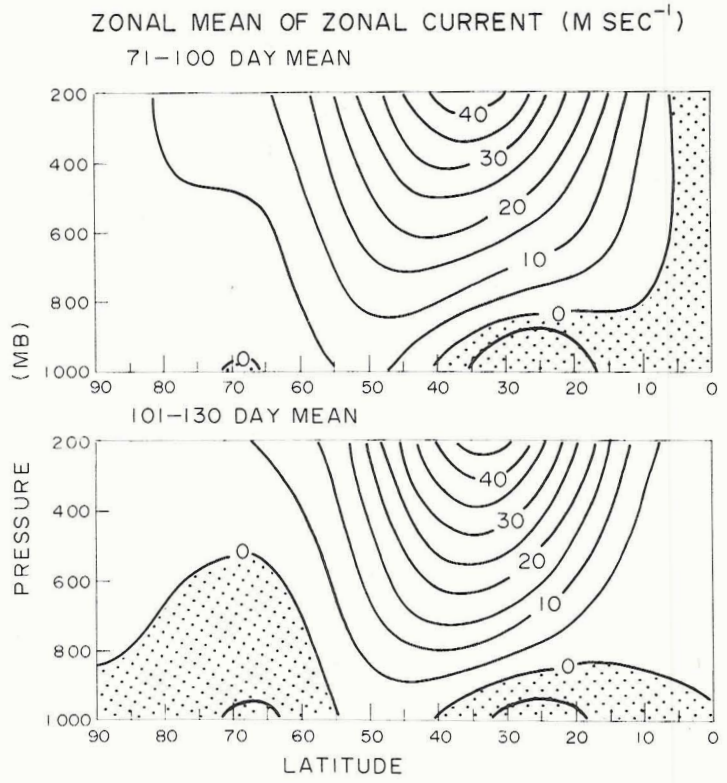

Fig. 15 - 30-day mean latitude-height distributions of the zonally averaged zonal wind (m/sec) for the periods of 71-100 days (upper part) and 101-130 days (lower part). Easterly regions are shaded.

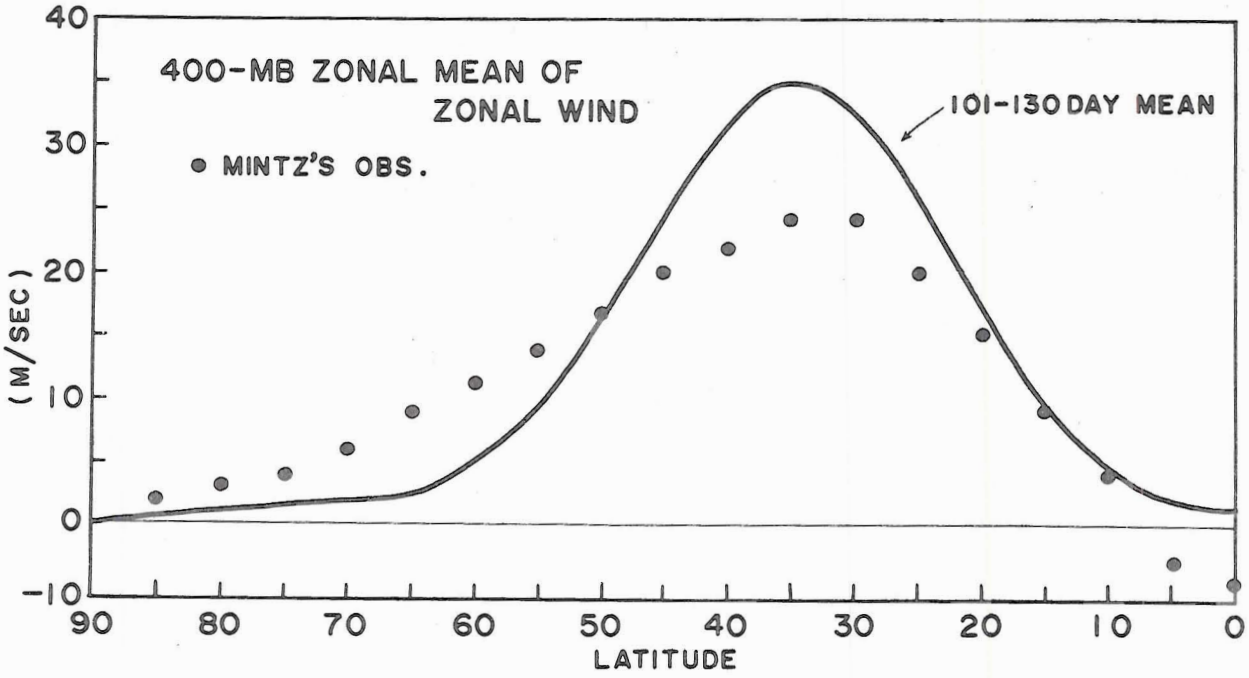

Fig. 16 - 101-130 day mean latitudinal distribution of the zonally averaged zonal wind (m/sec) at the 400 -mb level and corresponding winter mean values (solid circles) obtained by Mintz (1954).

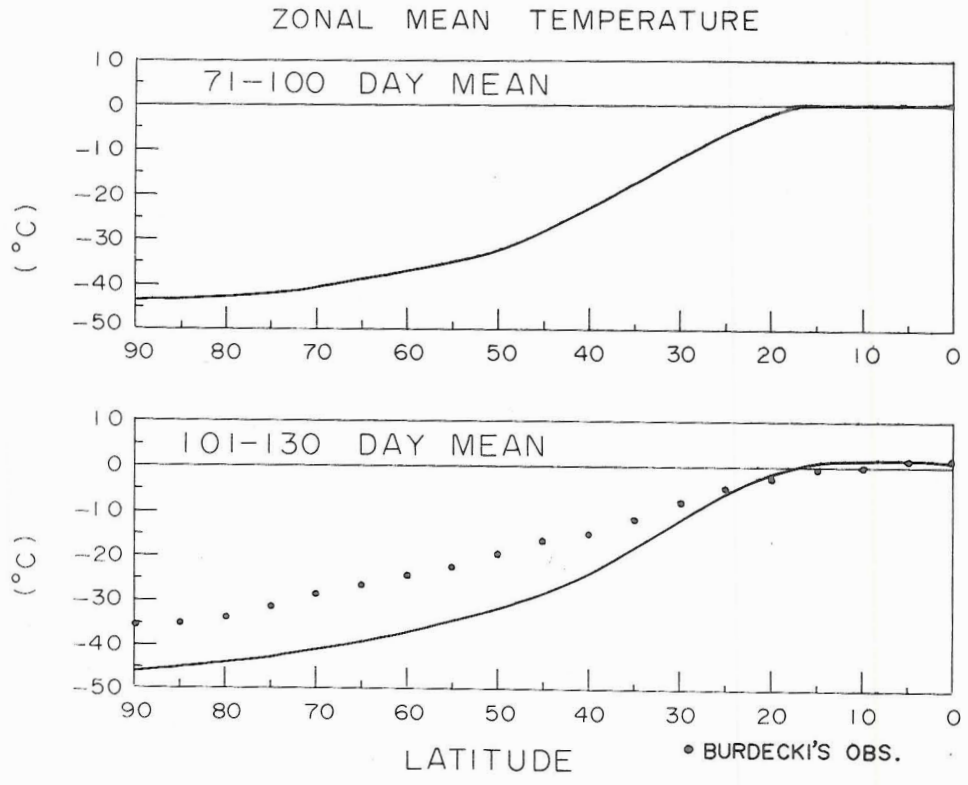

Fig. 17 - 30-day mean latitudinal distributions of the zonal mean temperature for the periods of 71-100 days (upper part) and 101-130 days (lower part). Solid circles show winter mean values obtained by Burdecki (1955).

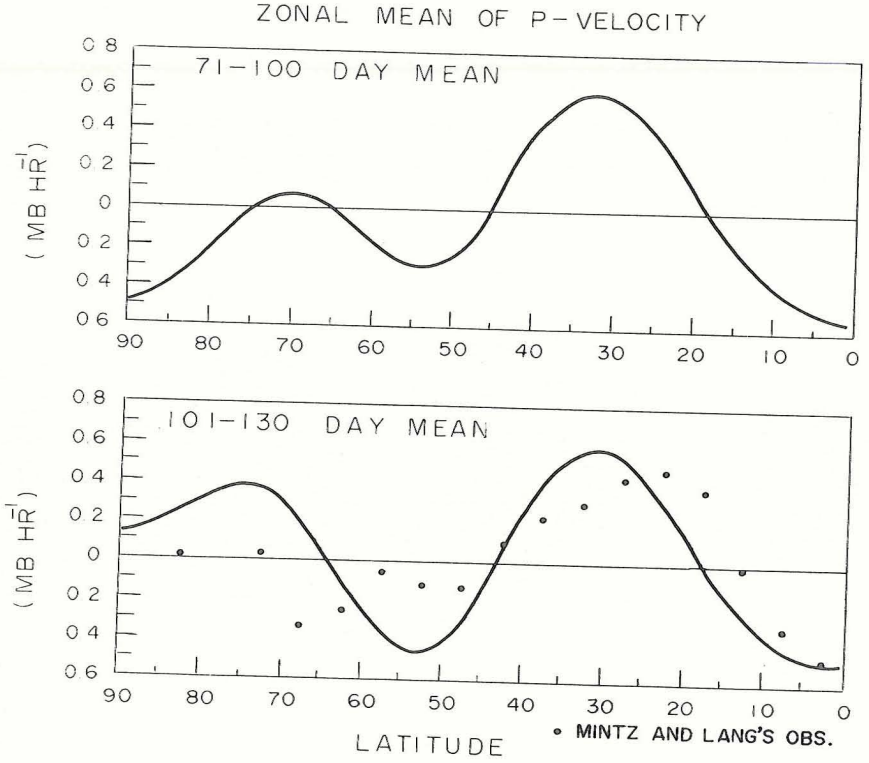

Fig. 18 - 30-day mean latitudinal distributions of the zonal mean vertical p-velocity (mb./hr.) for the periods of 71-100 days (upper part) and 101-130 days (lower part). Solid circles show winter mean values obtained by Mintz and Lang (1955).

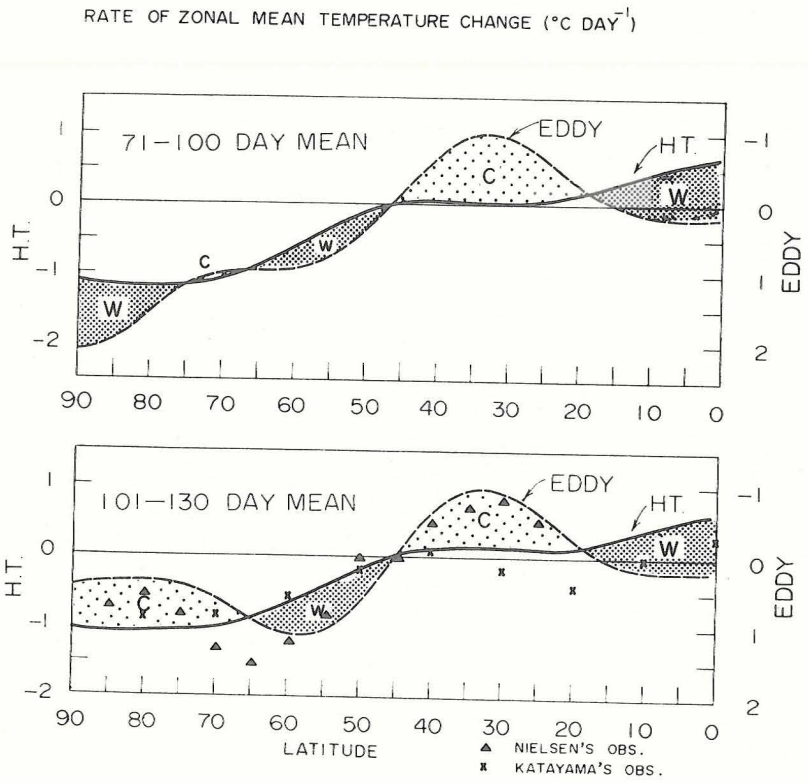

Fig. 19 - 30-day mean latitudinal distributions of the rate of the zonal mean temperature change due to diabatic heating (solid lines) and convergence of heat flux by large-scale eddies (dashed lines) for the periods of 71-100 days (upper part) and 101-130 days (lower part). January mean values obtained by Asakura and Katayama, 1964 (diabatic heating) and Wiin-Nielsen, Brown and Drake, 1963 (large-scale eddies) are plotted by cross and triangle symbols, respectively.

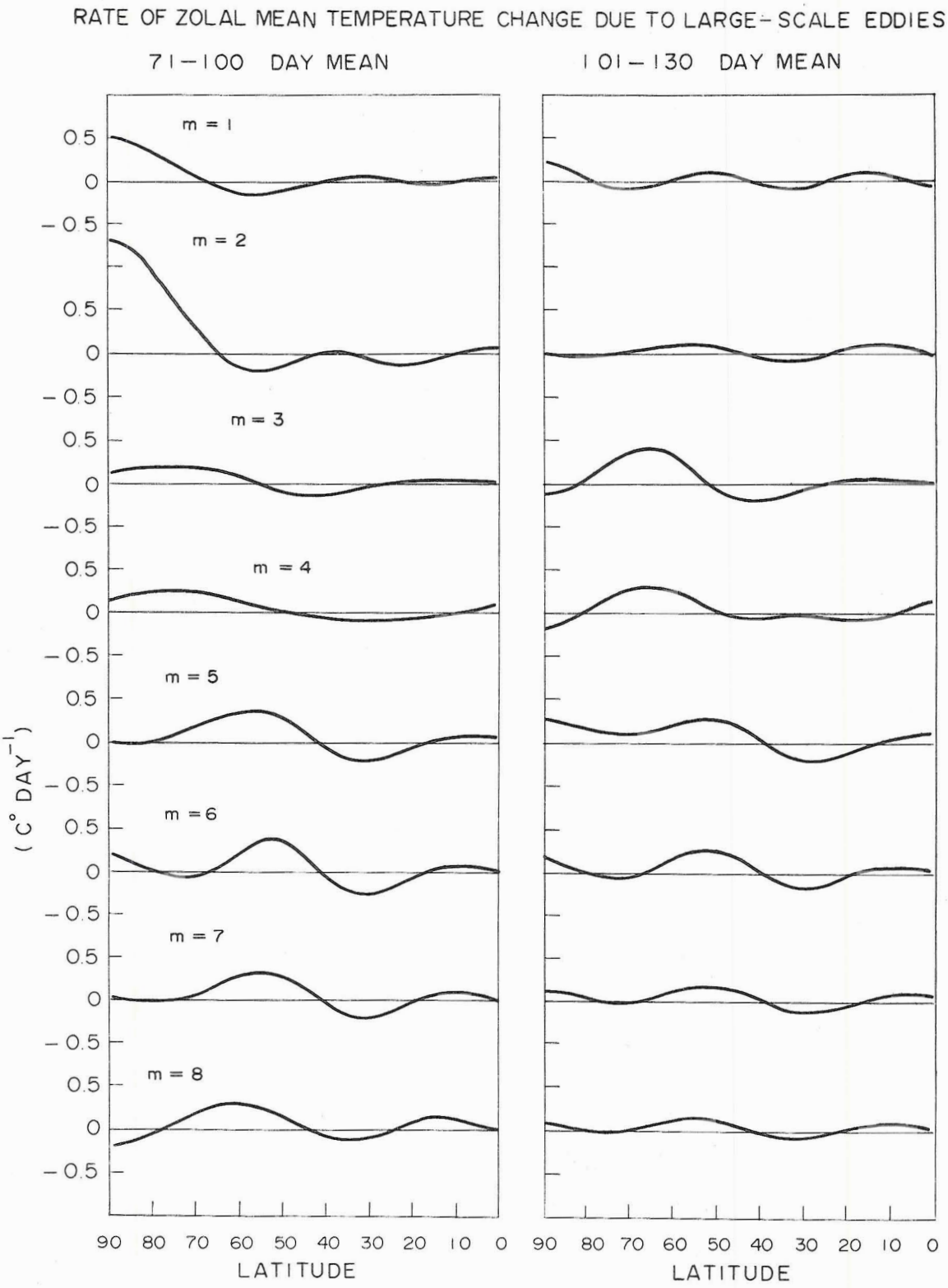

Fig. 20 - 30-day mean latitudinal distributions of the rate of the zonal mean temperature change due to convergence of heat flux for each of wave numbers 1 through 8, for the periods of 71-100 days (left part) and of 101-130 days (right part).

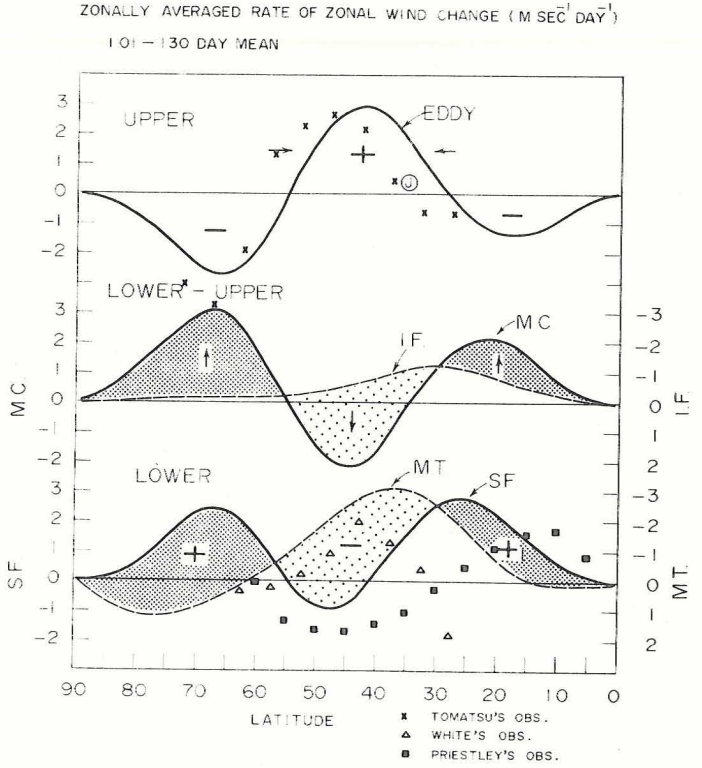

Fig. 21 - Mean latitudinal distributions of the rate of the zonal angular momentum change due to various components of angular momentum balance for the period of 101-130 days. Upper part: convergence of r.a.m. (relative angular momentum) due to large-scale eddies in the upper layer. Middle part: transports of r.a.m. from the lower to the upper layer due to the mean meridional circulation (MC) and vertical eddy diffusion (IF). Lower part: generation of r.a.m. due to surface (SF) and mountain (MT) torques. The corresponding observed values are shown by cross (EDDY), triangle (MT) and square (SF) symbols.

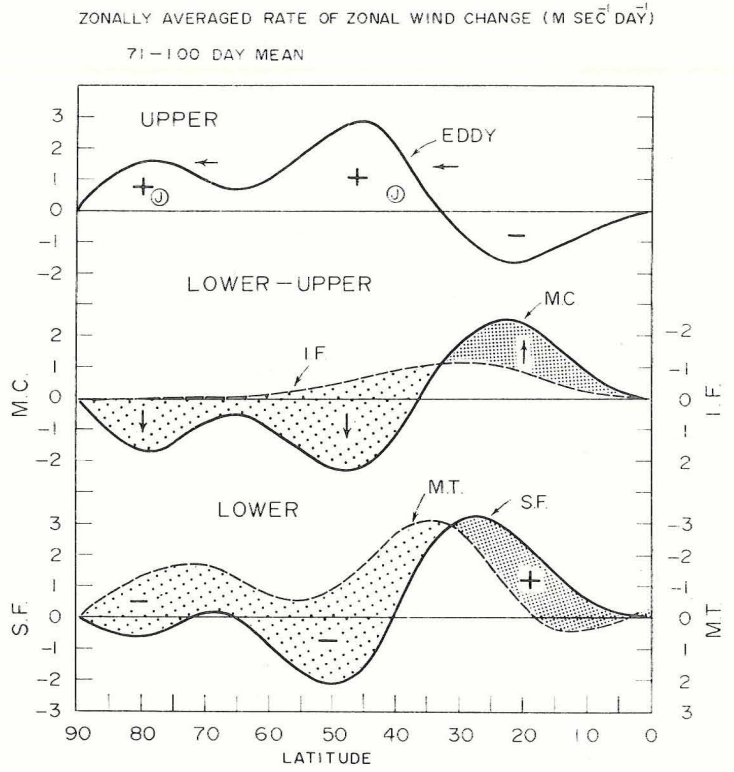

Fig. 22 - Same as Fig. 21, but for the period of 71-100 days.

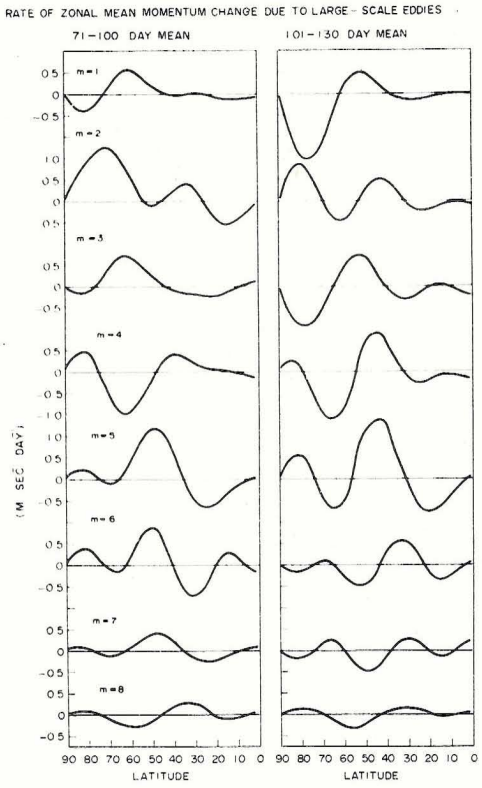

Fig. 23 - 30-day mean latitudinal distributions of the rate of the zonal angular momentum change for each of wave numbers 1 through 8 for the periods of 71-100 days (left part) and 101-130 days (right part).

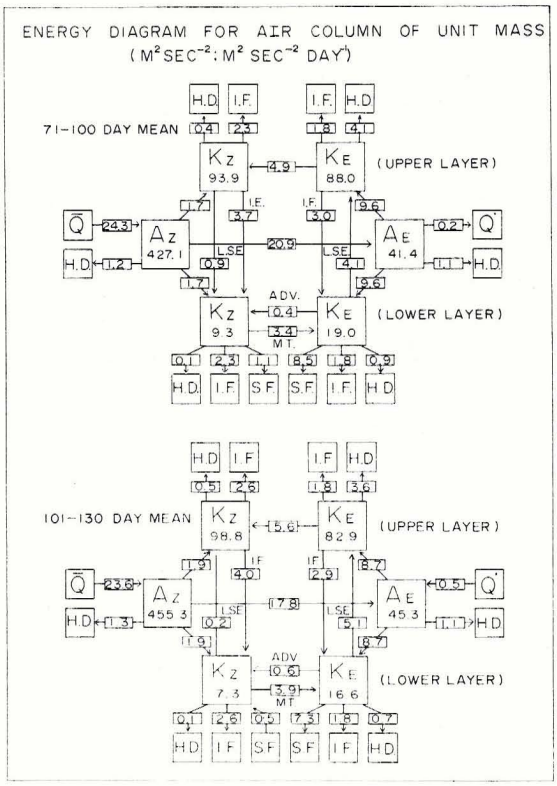

Fig. 24 - 30-day mean energy diagram for the air column of unit mass during the periods of 71-100 days (upper part) and 101-130 days (lower part). (Units: m^2sec^{-2} for energy, $m^2sec^{-2}day^{-1}$ for energy transformation).

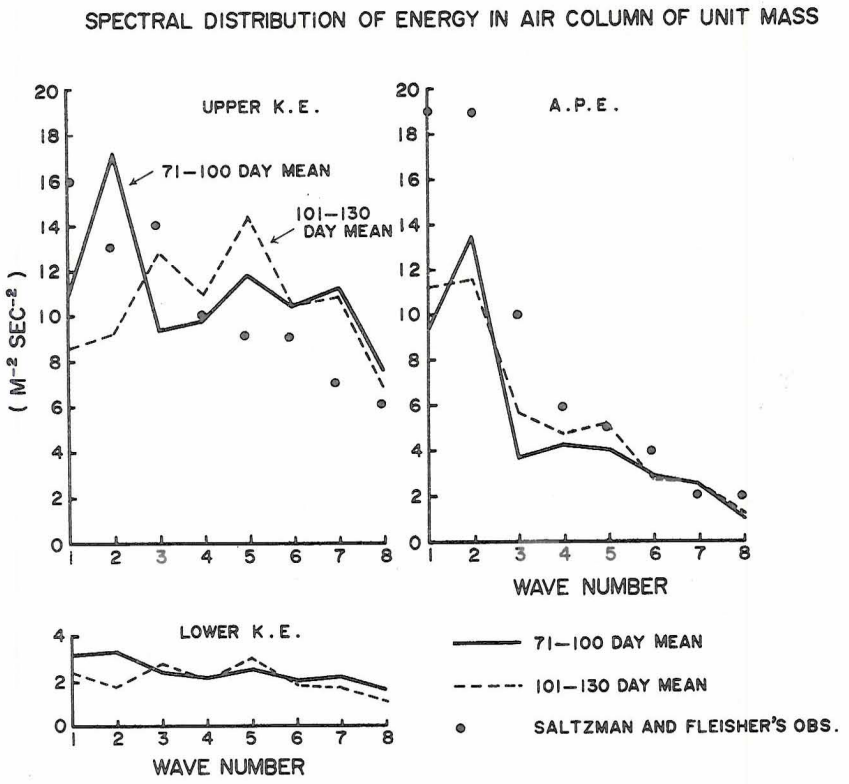

Fig. 25 - 30-day mean spectral distributions of kinetic energy in the upper layer (left upper part) and the lower layer (left lower part) and that of available potential energy (right part) for the air column of unit mass during the periods of 71-100 days (solid lines) and 101-130 days (dashed lines). Solid circles show winter mean values obtained by Saltzman and Fleisher (1961; 1962).

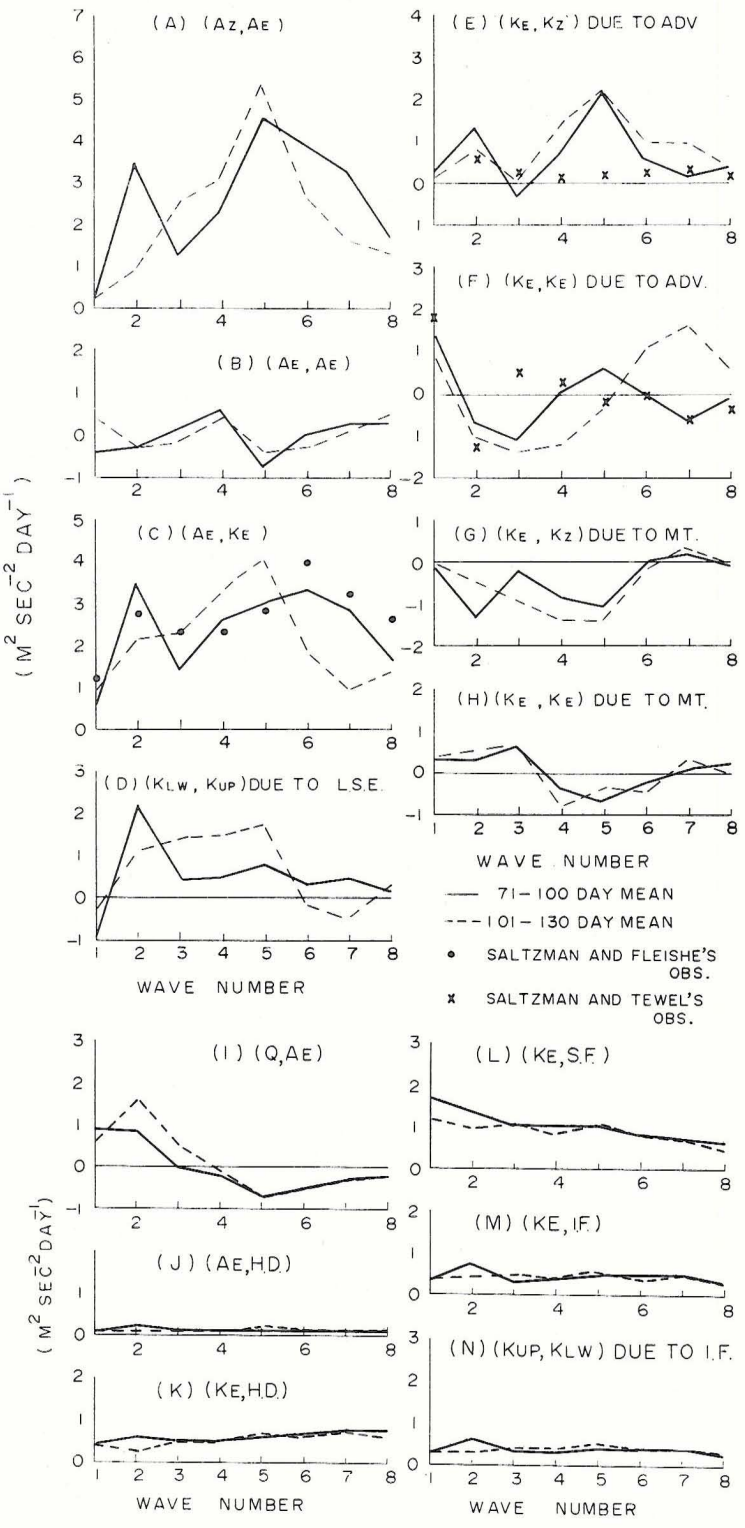

Fig. 26 - 30-day mean spectral distributions of energy transformation for the air column of unit mass due to various components for the periods of 71-100 days (solid lines) and 101-130 days (dashed lines). The observed values obtained by Saltzman and Fleisher (1961) and Saltzman and Teweles (1964) are also shown for comparison. (A): transformation from A_Z to A_E, (B): transformation of available potential energy among the disturbances, (C): conversion from A_E to K_E, (D): transfer of kinetic energy from the lower to the upper layer through the pressure force, (E): transformation from K_E to K_Z through the advective term, (F): transformation of kinetic energy among the disturbances through the advection term, (G): same as (E), but through the mountain effect, (H): same as (F), but through the mountain effect, (I): generation of available potential energy due to diabatic heating, (J): dissipation of A_E due to horizontal eddy diffusion, (K), (L), and (M): dissipations of kinetic energy due to horizontal eddy diffusion, surface friction and vertical eddy diffusion, respectively, and (N): transfer of kinetic energy from the lower to the upper layer through vertical eddy diffusion.

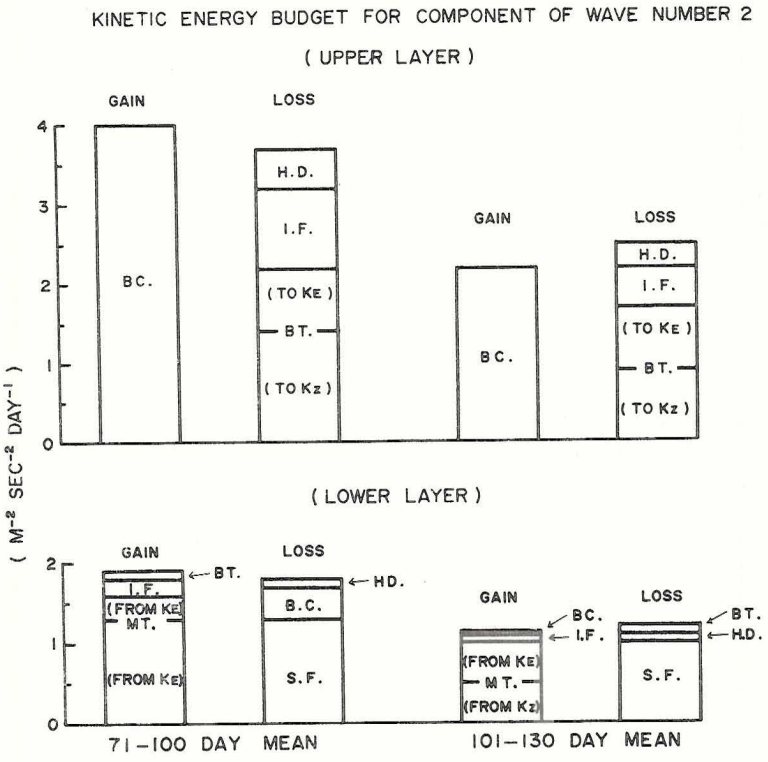

Fig. 27 - 30-day mean kinetic energy budget in the air column of unit mass for the disturbance of wave number 2.

COMPARISON OF ENERGY COMPONENTS ($M^2 SEC^{-2}$) AND ITS EXCHANGE ($M^2 SEC^{-2} DAY^{-1}$)

	Az	Ae	Kz	Ke	(Az,Ae)	(Ae,Ke)	(Ke,Kz)	(Kz,Az)	(Q,Az)	(Ae,Q)	(Az,Ds)	(Ae,Ds)	(Kz,Ds)	(Ke,Ds)
101-130 DAY MEAN OF COMPUTED RESULTS	455	45	106	100	17.8	17.4	6.2	-3.8	23.6	-0.5	1.3	1.1	5.3	15.2
OBSERVED RESULTS COMPILED BY OORT	400	150	80	70	25.9	19.0	3.5	0.9	26.8	6.9	—	—	4.3	15.6
SMAGORINSKY 9-LEVEL DRY MODEL	737	35	144	39	32.1	25.9	6.3	1.3	44.9	1.9	7.5	6.2	5.5	18.9
SMAGORINSKY 2-LEVEL MODEL	940	18	273	35	24.8	21.1	10.4	0.9	29.8	0.7	10.7	1.7	7.8	13.0
PHILLIPS 2-LEVEL MODEL	1190	25	272	68	30.0	30.0	12.8	3.4	21.0	0.0	2.6	0.9	8.2	7.7

Table 1 - Components of energy (m^2/sec^2) and energy transformation (m^2/sec^2 day) obtained by this experiment, the compilation of observed data by Oort (1964), and other numerical experiments [Smagorinsky, Manabe and Holloway (1965), Smagorinsky (1963), and Phillips (1956)].